https://doi.org/10.15407/ufm.26.03.626

O.I. DEKHTYAR 1,*, J. JANISZEWSKI 2,**, and P.E. MARKOVSKY 1,***

- ¹G.V. Kurdyumov Institute for Metal Physics of the N.A.S. of Ukraine, 36 Academician Vernadsky Blvd., UA-03142 Kyiv, Ukraine
- ² Jarosław Dąbrowski Military University of Technology,
- 2, Gen. Sylwester Kaliski Str., 00-908 Warsaw, Poland
- * dekhtyar@imp.kiev.ua, ** jacek.janiszewski@wat.edu.pl, *** pmark@imp.kiev.ua, pavlo.markovsky@gmail.com

PATTERNS OF THE MECHANISMS OF DEFORMATION AND STRAIN HARDENING OF TITANIUM ALLOYS AND METAL MATRIX COMPOSITES BASED ON THE ANALYSIS OF EXPERIMENTAL RESULTS ON QUASI-STATIC AND DYNAMIC COMPRESSIONS

The deformation behaviour of titanium-based alloys and their composites during quasistatic and high-strain-rate compressions is analysed based on the earlier method developed by V.F. Moiseev and his colleagues to analyse stress-strain curves obtained under tension. The present overview approach is employed for the treatment and subsequent analysis of numerous compression curves obtained from quasi-static and high-strainrate experiments with titanium-based alloys and their composites with varying compositions and initial microstructures. As shown convincingly, the Moiseev's method can also be successfully applied to analyse the behaviour of alloys under compression. A comparison of the obtained data with structural studies made it possible, in most cases, to identify the mechanisms of deformation and strengthening of titanium alloys in a wide range of compression rates. As found, depending on the type and morphology of the initial structure, deformation and strengthening under compression can be controlled by either α - or β -phase, or both phases simultaneously. The influence of the level of alloying with β-stabilizers and the introduction of strengthening dispersed high-modulus particles into the titanium matrix are considered. As revealed, the strengthening mechanism is often different under quasi-static and dynamic compres-

Citation: O.I. Dekhtyar, J. Janiszewski, and P.E. Markovsky, Patterns of the Mechanisms of Deformation and Strain Hardening of Titanium Alloys and Metal Matrix Composites Based on the Analysis of Experimental Results on Quasi-Static and Dynamic Compressions, *Progress in Physics of Metals*, 26, No. 3: 626–679 (2025)

© Publisher PH "Akademperiodyka" of the NAS of Ukraine, 2025. This is an open access article under the CC BY-ND license (https://creativecommons.org/licenses/by-nd/4.0)

sions. Moreover, in the case of high-strain-rate compression, the deformation behaviour can differ between the first stage and subsequent stages, which exhibit an oscillating nature. A physical explanation is proposed for the effects discovered during quasi-static and dynamic compressions of the considered titanium materials.

Keywords: titanium, titanium alloys, titanium-matrix composites, compression tests, quasi-static and dynamic deformations, mechanism of deformation.

1. Introductory Points: Analysis of the Deformation Mechanism from Stress–Strain Curves in Tensile Tests

The question of the mechanism of the deformation of metallic materials is one of the key issues both in purely scientific and practical terms. After all, it determines the mechanical behaviour of these structural materials in practical use because it ensures resistance against applied external loads, and hence the reliability of the operation of machines and structures made from them [1–3]. At the same time, deformation mechanisms also define the manufacturability of their processing by mechanical and thermomechanical treatments [4–6]. In the first case, the mechanical behaviour of materials is important and therefore studied in a wide temperature range from cryogenic to relatively high temperatures, while in the second case, predominantly at elevated temperatures.

The mechanical behaviour of metallic materials during deformation by various methods and under different conditions has been intensively studied for many decades. Most aspects of the deformation of metals and allovs are well studied both at the micro and macro levels. However, some special issues, such as the contribution/participation of individual phases of a multiphase material in deformation processes, have been studied to a lesser extent. However, for multiphase materials, this aspect is very important. When the constituting material phases differ in chemical composition and especially crystallographic structure (systems of easy slip directions and planes), the deformation in them occurs in different ways, deformation defects accumulate in different ways, and microcracks begin to appear at different stages, leading to the destruction of the material as a whole. In addition to differences in composition and crystallography, these processes are also influenced in a certain way by the microstructure of the material, as well as the test/loading scheme and the rate of application of the external load. Among the works devoted to the experimental study of the physical mechanisms of plastic deformation of pure metals, the works of V.F. Moiseev and co-authors [7, 8] should be especially noted. In these studies, mainly on metals with a b.c.c. lattice, it was shown that the homogeneous stage of tension of metals, represented in the co-ordinates 'true stress σ -true strain e', can be qualitatively analysed from the point of view of the phase-structural state of these metals. Namely, if the homo-

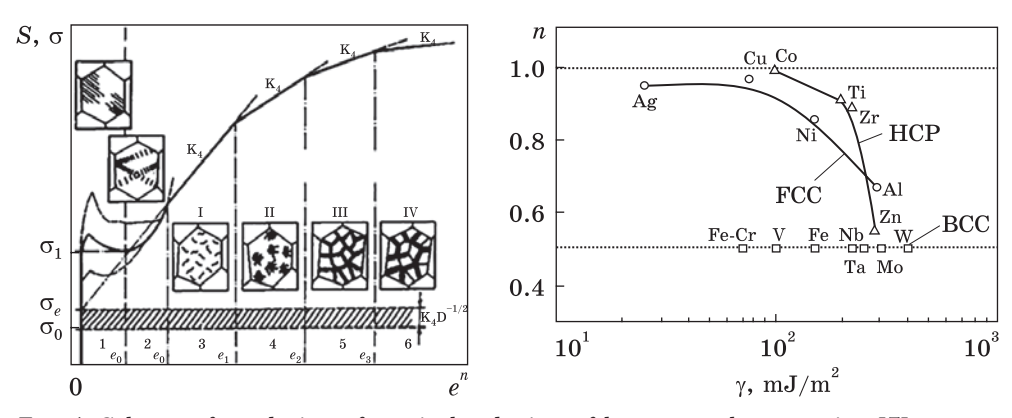


Fig. 1. Scheme of gradation of strain hardening of b.c.c. metals at tension [7] Fig. 2. Dependence of the strain hardening exponent n on the stacking fault energy γ for metals with different types of crystal lattice: b.c.c., f.c.c., and h.c.p. [9]

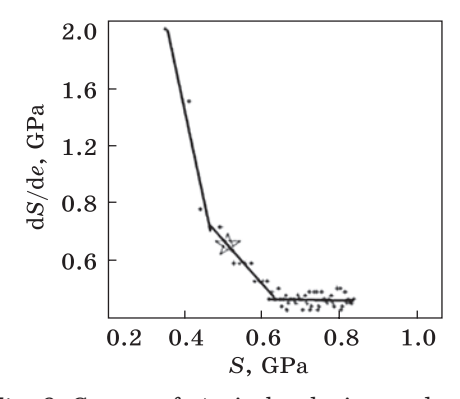
geneous stage of the tensile curve is presented in the form

$$\sigma = \sigma_{0.2} + \sum_{s=1}^{m} K_s (e_s - e_{s-1})^n$$
 (1)

 $(\sigma_{0,2}$ is the stress that includes the quasi-elastic section of the hardening curve and the stress corresponding to the plastic deformation of 0.2%, K_s is the strengthening coefficient, n is the strengthening index, s is the sequence number of the section of the strengthening curve), then the homogeneous stage in the coordinates $\sigma - e^n$ is divided into a number of consecutive rectilinear sections for a certain specific value of n (Fig. 1) In this case, the deformation values e_s and e_{s-1} correspond to the end and beginning of a specific section numbered s, which varies from 1 to m. As a result of numerous experiments, it was established that each of these areas corresponds to a certain type of dislocation structure and is characterized by its strengthening coefficient. As a rule, a homogeneous stage of annealed metal with a low initial density of defects is divided into three rectilinear sections. The initial region corresponds to randomly distributed dislocations that control the deformation mechanism at this stage of deformation. The second section corresponds to the formation of heterogeneous dislocation clusters. The third section corresponds to the formation of a cellular structure with virtually non-oriented cell boundaries. The approach of Moiseev and his colleagues was applied primarily to the initial stages of strengthening [7, 8].

The undoubted advantage of such processing is its sensitivity to structural rearrangements that occur in the early stages of deformation, and the ability to classify the laws of structure formation depending on the stacking fault energy and the type of crystal structure (Fig. 2) [9].

A similar approach regarding f.c.c. metals, which well describes the later stages of hardening, was developed in Ref. [10] by Cox and Meking,



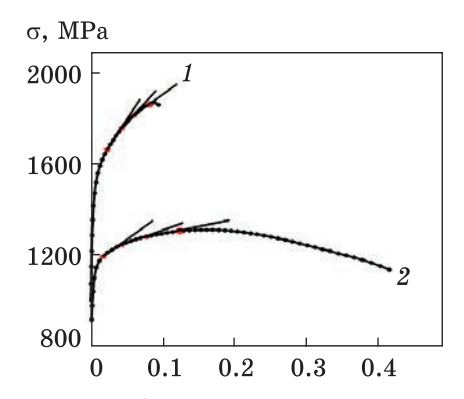


Fig. 3. Curves of strain hardening under compression of Armco-iron [10] Fig. 4. Tensile strain hardening curves of Ti-8Al-1.4Si-2.2Zr alloy: n = 0.93 (1) and 0.59 (2) [16]

who, in addition to tension, also considered hardening under quasi-static compression (Fig. 3).

Studying the tension and compression curves of metals with different crystal structures, it was established [7–10] that each crystal lattice has its own value of the strengthening exponent n. Thus, the h.c.p. lattice is characterized by the strengthening exponent n = 0.6-1; the b.c.c. lattice is characterized by n close to 0.5.

This question also concerns such an important structural material as titanium and its alloys. Most commercial titanium alloys are used in a two-phase state, when the material consists of alpha (h.c.p.) and beta (b.c.c.) phases that differ significantly in symmetry and the presence of easy dislocation glide planes [11, 12]. In Refs. [13–18], the above approach was also applied to titanium two-phase alloys, where the deformation mechanism, depending on the structural-phase state, can control both alpha and beta phases.

For example, in Ref. [16], it was shown that tensile strain hardening curves of Ti-8Al-1.4Si-2.2Zr alloy are characterized by different values of n in dependence of in what phase, alpha (n=0.93) or beta (n=0.59) this alloy was deformed and what structures were formed (Fig. 4). Curve 1 was obtained for alloy with lamellar structure with elongated α -grains and β -layers. Curve 2 was obtained for an alloy with a fine-grained equiaxed α -Ti structure. Tangents on the curves corresponded to the s sections with different kinds of structures in accordance with Eq. (1).

Compressive testing of metal materials is no less important than tensile tests since, in most cases, the compressive component of the loads also occurs in the actual operating conditions of products. Considerable attention was paid to such tests of metals and the study of deformation mechanisms, especially at high temperatures, since this was the scientific basis for optimizing the modes of their thermomechanical treatment [19–23].

As for compression tests at lower temperatures (primarily room temperature), conclusions about the features of the deformation mechanism were made mainly based on the microstructure of metals formed as a result of the test [24–26]. In addition, special attention was paid to the influence of the strain rate since the transition from quasi-static conditions to dynamic ones significantly affects the change in the nature of the deformation processes occurring in this case.

For titanium and alloys based on it, a fairly large number of works have been carried out to date, devoted to studying the effect of strain rate during compression tests [27–30]. Particularly, this topic was devoted to a series of works carried out together by scientists from G.V. Kurdyumov Institute for Metal Physics of the N.A.S. of Ukraine (Kyiv, Ukraine) and Jarosław Dabrowski Military University of Technology (Warsaw, Poland) [31-35]. In these studies, the influence of chemical and phase compositions, the type of crystallographic lattice, and microstructure on the mechanical behaviour of various titanium alloys depending on the compression strain rate was systematically investigated. Our previous work made a first step in the evaluation of peculiarities of the deformation mechanism of Ti-6Al-4V alloy with globular microstructure during compression with different strain rates [36]. In this paper, an attempt to apply the approach of analysis of strain hardening curves concerning several titanium alloys and metal matrix composites on their base at room temperature under both quasi-static and high-strain-rate dynamic compression was made. At the same time, for an adequate assessment of deformation mechanisms, the analysis of curves was performed in comparison with structural studies. It should be noted that such an analysis of the hardening curves under dynamic compression was applied for the first time in world practice.

2. Analysis of Deformation Mechanisms Based on the Stress–Strain Curves in Compression Tests

2.1. Some Key Features of the Test Method Used

Deformation with different strain rates makes it possible to reveal most fully the mechanisms of plastic deformation and their change depending on the structural-phase factors that describe the material itself and on the kinetic-force conditions of its external loading, which determine the course of accommodation processes in the material. Deformation under quasi-static conditions (in this case, quasi-static compression—QSC) can be performed on standard machines for mechanical testing, produced in a wide range and by various companies. But for dynamic tests, in addition to the usual tests for crack resistance, the high-strain-rate compression approach was proposed and realized in the form of a split Hopkinson pressure bar (SHPB), also called a Kolsky bar technique [37–39], which re-

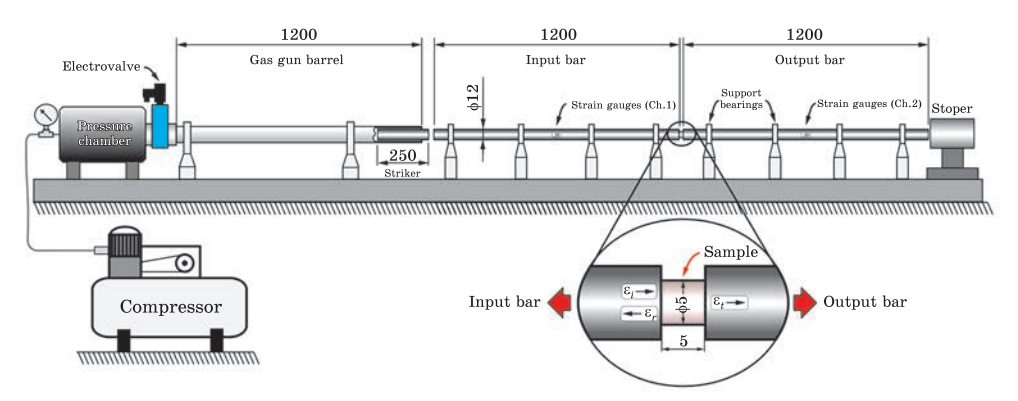


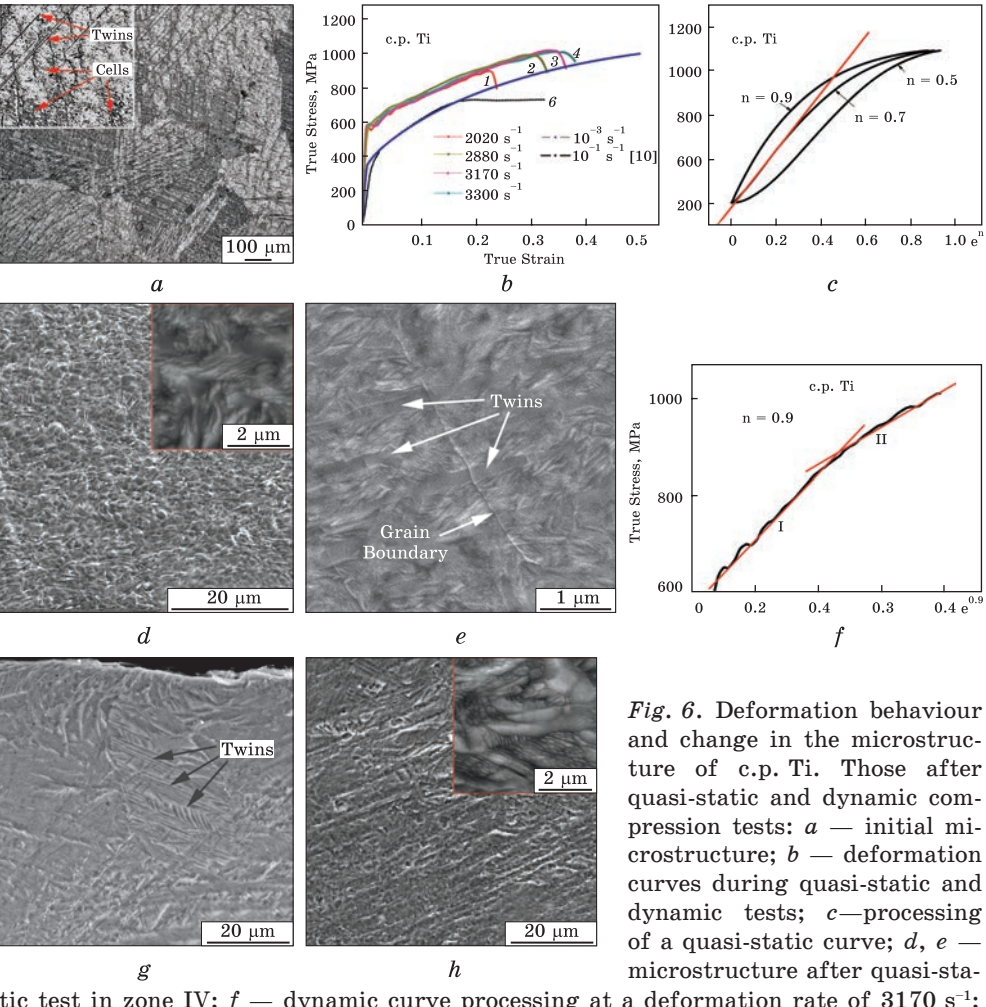
Fig. 5. The schematics of the split Hopkinson pressure bar (SHPB) system [31]

quires the individual manufacture of each such installation, as a rule, by the researchers themselves. The basic parameters of such an SHPB system are shown in Fig. 5. The length of the input and output bars was 1200 mm, the length of the striker bar was 250 mm, and the diameter of all bars was 12 mm. The bars were made of maraging steel (heat-treated MS350 grade). The striker bar was driven by a compressed air system with a barrel length of 1200 mm and an inner diameter of 12.1 mm. The impact striker bar velocities applied during the experiments were in the range from 10 to 25 m/s, which ensures strain rates in the range of 1100–3320 s⁻¹ for the dimensions of the used specimens. More details about equipment and basic principles of the technique employed are described in Refs. [31–35].

2.2. Commercial Purity Titanium (c.p. Ti)

Commercial purity titanium is a single-phase metal with a minimum total (not more than 0.4 wt.%) impurity concentration and an h.c.p. crystal lattice. The usual microstructure of industrial rolled products in the case of stabilizing annealing is characterized by equiaxed grains of the α -phase, which may have an internal substructure. For instance, Fig. 6, a illustrates the presence of numerous small cells and twins inside relatively large (above $400-500~\mu m$) α -grains. Interestingly, such a state is characterized by almost similar curves of strain hardening under compression both in quasi-static conditions (compression strain rate $10^{-3}~\rm s^{-1}$) and in dynamic test conditions (strain rate $>\!2200~\rm s^{-1}$) (Fig. 6, b). The difference is that the dynamic curves have fluctuations, while the quasi-static curve is very smooth, and the plasticity of technically pure titanium under quasi-static conditions is significantly higher than the plasticity under dynamic conditions. However, despite the similarity of the curves, the mechanisms of strain hardening in these two conditions are significantly different.

For the initial stage of the strain hardening curve of pure titanium in a quasi-static state, the most likely value is n = 0.7 (Fig. 6, c), which, in prin-



tic test in zone IV; f — dynamic curve processing at a deformation rate of 3170 s⁻¹; (g, h) — microstructure after dynamic testing in zones I (g) and II (h) [31]

ciple, is more characteristic of the simultaneous influence of the α - and β -phases (the latter is absent in this alloy). However, as is known, titanium with a single-phase h.c.p. lattice can be easily deformed at rather low temperatures due to twinning [1, 30, 31], which may even dominate the dislocation contribution. The microstructure of c.p. Ti after mechanical compression tests in quasi-static mode (Fig. 6, d) looks uniform in all zones. It is modified by plastic deformation, which causes a higher density of deformation defects and a smaller size of cells and twins. Numerous traces of plastic deformation in the form of slip bands, twins, and well-developed substructure within the α -phase are observed throughout the specimen. It should be noted that the representation of the deformation curve in σ - e^n co-ordinates is characterized by the presence of only one (the first) straight section (Fig. 6, c).

The rest of the curve shows a non-linear character in these coordinates. This may mean the extraordinary nature of strain hardening at the homogeneous stage. The reason for this effect is not clear. However, it can be assumed that it may be related to secondary twinning within primary twins, which can be distinguished in Fig. 6, e. From this point of view, the presence of a linear section in Fig. 6, c may indicate that secondary twinning does not begin at the very beginning of homogeneous deformation, but a little later. At the same time, the deformation twins differ from those in the initial state (Fig. 6, a), and the dislocation cells significantly decrease in size during compression. However, the changes in the dislocation structure, as we can see, are reflected in the strain-hardening curve within our current understanding of the physics of compression deformation: an increase in the total density of dislocations leads to a slowdown in the rate of strength growth. Regarding the value of the strengthening index n = 0.7, which is characteristic of the strengthening mechanism associated with the action of interphase α/β -boundaries, when both α- and β-phases act as a strengthening factor to an approximately equal extent, an important assumption must be made. It is very likely that in this case, when only the α -phase exists, the role of the other phase is played by the volume of the twin, and the boundary of the twin plays the role of an interphase boundary.

During the dynamic compression, there is a significant increase in the density of deformation defects, while the general nature of the substructure (Fig. 6, g, h) remains approximately the same as in the initial undeformed state (Fig. 6, a) in all zones, i.e., close to the contact surfaces of the specimen with the rod (Fig. 6, g), as well as throughout the specimen (Fig. 6, h). Given that titanium with a single-phase h.c.p. lattice could be easily deformed due to twinning at rather low temperatures [1, 30, 31], it was expected that the defect areas should contain mostly twins. However, bearing in mind the possibility of a significant local-temperature increase during deformation [32, 40, 41], several other scenarios should not be excluded, namely the formation of a well-developed dislocation substructure and the possibility of phase transformations, even the formation of martensite, as reported in Ref. [31], where c.p. Ti was subjected to rapid heating and cooling. Finally, due to the high plasticity of c.p. Ti the introduction of some deformation defects for this alloy as a result of specimen preparation (even after delicate ion polishing and/or etching) could not be completely ruled out, although their presence creates a 'background' effect in all specimens of this alloy. Nevertheless, zones of localized deformation and ASB were not detected in specimens c.p. Ti, even when tested at the highest strain rates (Fig. 6, g, c).

At the same time, the mechanism of strain hardening during the process of ultra-high strain rate compression (Fig. 6, e) is significantly different from the case of quasi-static compression. The stage of uniform

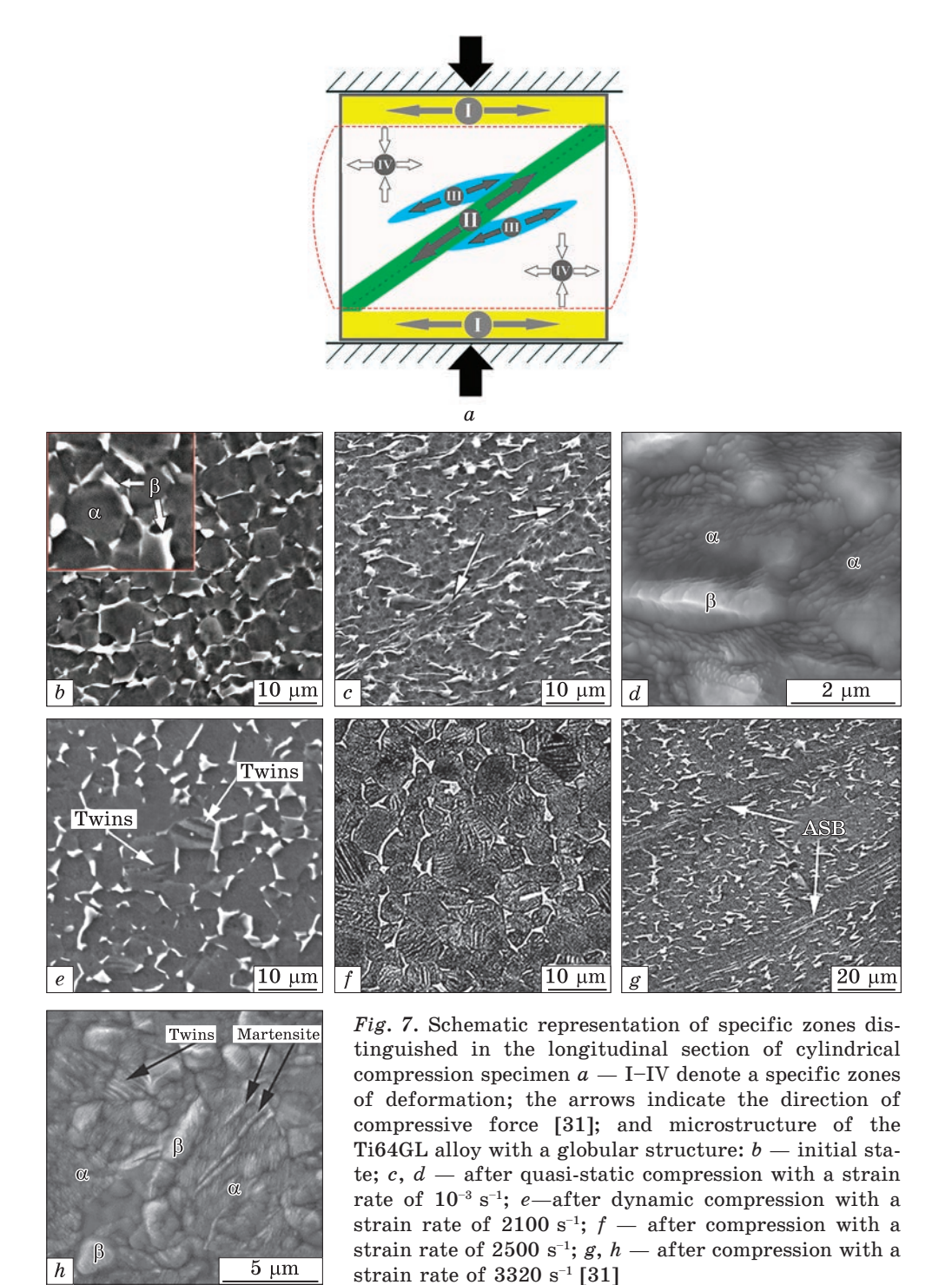
deformation is characterized by a constant exponent of n=0.9, but two areas with different coefficients of strain hardening. Most likely, the first section is related to the deformational development of the cellular structure due to the sliding of dislocations (shear), and the second to the rotational mode of deformation caused by the movement of twins. The strengthening index n=0.9 indicates that, and this is natural, the mechanism of strain hardening is controlled only by the α -phase, since twins in this case cannot perform the role of the second phase.

2.3. Two-Phase $\alpha + \beta$ Ti-6(wt.%) Al-4V (Ti64) Alloy

Ti64 is an alloy most widely used for different applications in comparison with other commercial titanium alloys, due to which it even received the name 'workhorse' of the titanium industry [12]. Different methods and regimes of thermomechanical and heat treatments form a rather wide range of microstructural states, which significantly differ in mechanical properties. It is generally accepted that the best balance of strength and plastic properties occurs when tensile-tested material has a dispersed microstructure with a globular morphology of the α -phase [12, 42].

2.3.1. Ti64 Alloy with Globular Initial Microstructure (Ti64GL)

It was shown in many studies that the globular microstructure of Ti64 alloy has significant superiorities over other microstructural states in many properties, firstly tensile ductility, which is well balanced with strength [12, 42]. Moreover, some ballistic investigations of this material also showed its better resistance as compared with the lamellar state that is characterized by better crack propagation resistance [43]. In our previous work, it was found that the globular microstructure of the Ti64 alloy has a significant superiority not only over the lamellar microstructure of the same alloy but also over many other titanium alloys in mechanical characteristics and in dynamic tests [31, 36]. Moreover, taking into account the specific weight, and over some other structural metal materials, in particular, even over armoured steels of the ARMOX type. In Refs. [31, 44] it was hypothesized that the advantage of the globular microstructure over the lamellar microstructure of the same material, as well as over single-phase α - or β -titanium alloys, may be associated with the peculiarity of the interphase boundaries: both their type and the geometry and crystallographic misorientation of neighbouring crystals. However, this hypothesis has caused some criticism from experts. Therefore, in Ref. [31], the first attempt was made to evaluate from the point of view of the analysis of compression strain curves at different strain rates in their direct connection with a detailed analysis of the post-deformation microstructure of the compression-tested Ti64 alloy with a globular microstructure. The general evolution of the microstructure during such tests is shown in



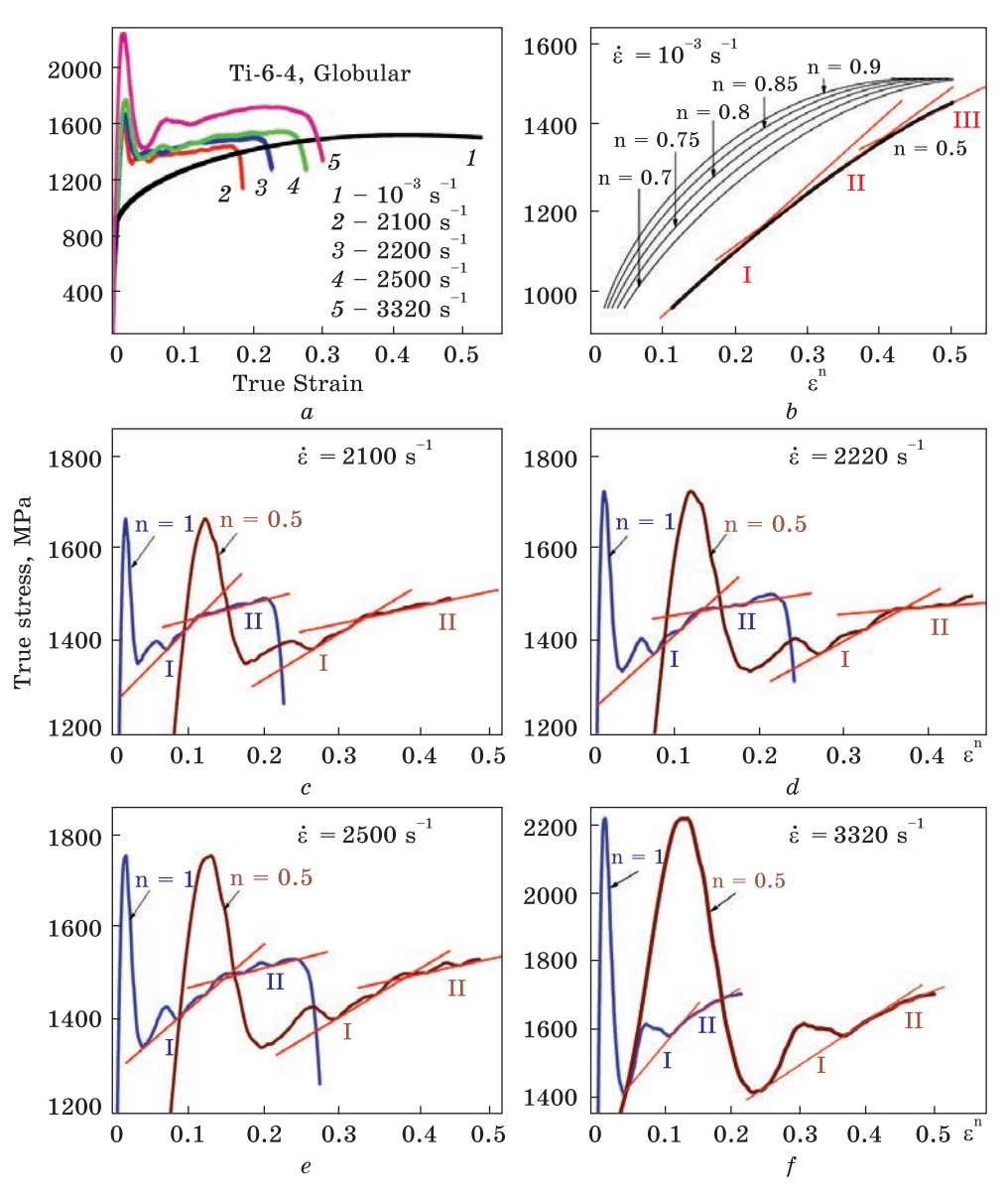


Fig. 8. Analysis of homogeneous sections of compression curves of Ti64GL alloy deformed at different strain rates: a — output curves in true stress—true compression strain [31]; b — the result of presentation of quasi-static compression curves with a strain rate of 10^{-3} s⁻¹; c-f — the result of presentation of dynamic compression curves with different strain rates [36]

Fig. 7. Now we present not only the data from the above works, but also supplement them with a new detailed analysis.

First of all, the phase-structural state obtained by preliminary hardening and characterized by a clear globular structure was chosen as the ob-

ject of compression deformation tests and further microstructure research: α -grains are surrounded by layers of β -phase (Fig. 7, a). In this state, the Ti64GL alloy has the highest strength with good plasticity. This structure was the starting point for further quasi-static and dynamic compression tests. Figure 7, b-g shows how it changes during compression at different strain rates. It should be noted that one of the main features of the structure after dynamic tests is the appearance of twins in the α -phase (Fig. 7, d-g) of different densities depending on the compression velocity. That is, at very high compression rates, twinning is manifested as one of the mechanisms of deformation. In turn, this means that one of the components of deformation is the rotational mode of deformation.

Some true stress—true strain curves for compression of these Ti64GL samples are shown in Fig. 8, a. Figure 8, b presents the result of the analysis of the hardening curve of the Ti64GL alloy with a globular structure under quasi-static compression at a rate of 10^{-3} s⁻¹ at different values of n. It turned out that the most adequately homogeneous stage of the hardening curve is described by three straight sections at n = 0.5. By analogy with tension, it can be assumed that the mechanism of strain hardening in compression is most likely controlled by the β-phase, in contrast to tension, when the α -phase is decisive [13, 14]. Comparison of this fact with the results of scanning electron microscopy (SEM), namely with the original structure (Fig. 7, b) and the structure formed during compression (Fig. 7, b, c), confirms the determining role of the β -phase in the mechanism of strain hardening of the Ti64GL alloy under quasi-static compression. Moreover, the β -phase is, in fact, the boundary of the globules both in the initial state (Fig. 7, a) and after deformation by compression (Fig. 7, c). Moreover, the nature of the dislocation structure after compression indicates that the main deformation occurred in the α-phase (Fig. 7, d), and the β -phase was an effective barrier to dislocation slip from the α -phase. In addition, by analogy with tension, it can be assumed that at the initial stage, randomly distributed dislocations act; at the second stage, tangles and clusters of dislocations are formed, and at the third stage, a cellular substructure with non-oriented cell boundaries is formed in the α -phase (Fig. 7, c).

A completely different picture and other regularities of compression deformation are revealed during dynamic tests (Fig. 8, c-f). First, we note that the strain hardening curves under dynamic compression have an oscillating character with fairly clear minima and maxima (Fig. 8, a). It is quite likely that during a dynamic impact, both a deformation wave associated with plastic deformation and a sound wave associated with elastic oscillations of crystal lattices occur. In line with the above, an analysis of the deformation curves of the Ti64GL alloy under dynamic compression was performed (Fig. 8, c-f). The straight lines on the sections of the curves in the $\sigma-e^n$ co-ordinates were drawn according to the minima,

which should correspond to the stress relaxation points during the deformation process.

First, we note that the decomposition of the curves for the strain rates of 2100, 2220, 2500, and 3320 s⁻¹ looks almost identical. For all rates of hardening in the homogeneous stage, it is described in the same way with the hardening exponent n in a wide range from 0.5 to 1, and in all cases, two straight sections are distinguished. The observed fact of the simultaneous description of curves with different values of n is quite unusual and differs from what happens for titanium alloys during quasi-static tension [5-10]. In quasi-static tension, as well as in quasi-static compression, all mechanisms that determine strengthening are associated with dislocations, that is, with shear deformations. Therefore, in this case, a hierarchical change in dislocation structure types, when one strengthening structure arises from another, is quite natural. Therefore, the strengthening mechanism is described, as a rule, by a single strengthening exponent n associated with a certain phase that controls this strengthening. A similar pattern is observed in our case of quasi-static compression (Fig. 6, b). In similar conditions of deformation in pure titanium, in addition to dislocations, twins were also observed [41]. In our alloys, active deformation with a rotational mode (twins) appears only during dynamic compression. Moreover, the density of twins increases very quickly with increasing compression rate, and they are observed in both α - and β -phases (Fig. 7, d). It is obvious that along with the deformation provided by the twins, shear deformation is carried out. This is evidenced by the presence of two straight sections in all cases. It is clearly visible that the last second stage of strengthening is associated with the formation of a dispersed cellular substructure, which is very well manifested in both the α - and β -phase (Fig. 7, g). Therefore, by analogy with the case of stretching, it can be assumed that the previous first stage is associated with the formation of a high density of dislocation clusters, which are transformed into dislocation cells at the second stage. It follows from the conducted analysis that the dynamic deformation, which is provided by both dislocations and twins, is indicated by the same description of the homogeneous stage of the exponent n in a wide range from 0.5 to 1. In connection with the above, the following hypothesis is proposed. At high deformation rates, centres of high stresses appear at the α/β -boundary due to the local accumulation of retarded dislocations. These stresses relax due to the formation of twins. In turn, twins provoke bulk rotational deformation, which causes the arrangement of b.c.c. and h.c.p. lattices, similarly to the coherent one. As a result, conditions are created for almost unimpeded slipping of dislocations from one phase to another. Thus, both phases give practically the same contribution to the deformation. Future research is needed to confirm or refute this hypothesis.

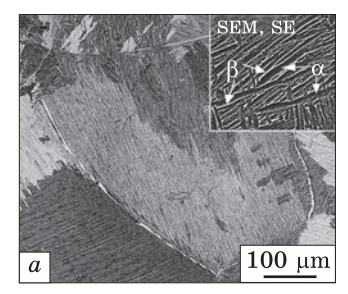
It should be noted that with an increase in the strain rate, the first minimum constantly approaches the first straight section and coincides with it at strain rates of 2500 and 3320 s⁻¹. We still do not have an explanation for this fact.

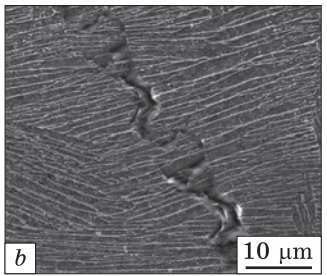
Thus, the dynamic compression of the Ti64GL alloy with a globular structure is characterized by the fact that both α - and β -phases control strain hardening simultaneously (as evidenced by the values of the hardening exponent n from 0.5 to 1). Deformation is provided by both dislocations (shear) and twins (rotation). In the future, it will be clarified whether this situation is characteristic only of the globular microstructure or of other structures as well.

2.3.2. Ti64 with Lamellar Initial Microstructure (Ti64LM)

This type of microstructure is usual for as-cast or heat-treated at temperatures of single β-phase conditions, and is characterized by worse than globular one balance of strength and ductility, but has some superiority in creep, and crack propagation resistances [12, 42]. The lamellar microstructure of the Ti64 alloy represents alternating α -plates and thin β -layers appear on cooling from the temperatures of the single-phase β -field in the form of colonies within rather coarse β -grains (Fig. 9, a). During dynamic compression tests, stress distribution zones appeared in the samples that were the same (Fig. 7, a), however, changes in the microstructure were noticeably different. For instance, cracks at the stage of fracture at high strain rate propagated across the plates in both zone II and IV (Fig. 9, b, c). This indicates that both α -plates and β -layers can be effective barriers to both dislocation movement and crack propagation. It should also be noted that some features in the course of the strain-stress curves (Fig. 10, a), which, in comparison with the globular microstructure (Fig. 8, a), primarily consist of a significant decrease in plasticity and destruction of the samples at lower strain rates.

The typical true stress—true strain curves for Ti64 with lamellar microstructure compressed with different strain rates are shown in Fig. 10, a. The homogeneous stage of the strain hardening curve of the Ti64LM alloy under quasi-static compression is characterized, firstly, by a strain hard-





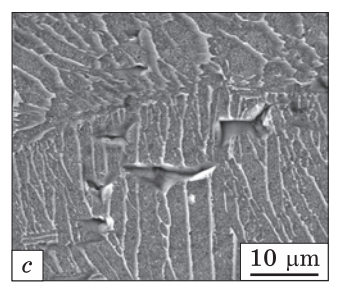


Fig. 9. Microstructure of the Ti64LM alloy specimen after dynamic tests of 1390 s⁻¹: a — general view; b — zone II; c — zone IV in the Fig. 7, a [31]

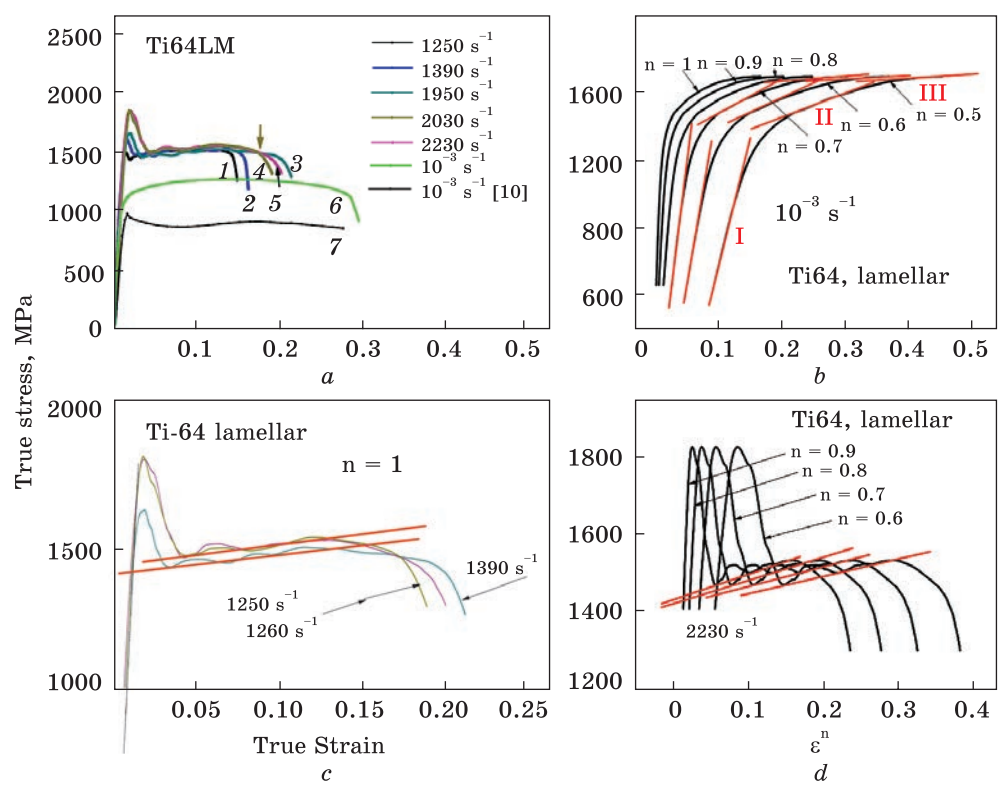


Fig. 10. Analysis of homogeneous sections of compression curves of Ti64LM alloy deformed at different rates: a — original curves in true stress coordinates—true compression strain [31]; b — the homogeneous part of the quasi-static compression curve at different values of n; c-d — result of representation of dynamic compression curves with different rates of deformation

ening exponent varied from 0.5 to 0.7, and secondly, by three straight sections in σ - e^n co-ordinates (Fig. 10, b). This means that the deformation mechanism is controlled mainly by β -phase interlayers and is fundamentally different from the mechanism when, during quasi-static tension, strengthening is controlled by α -plates [5–10]. At the same time, the deformation process has a shear character, and the microstructure develops sequentially from randomly distributed dislocations (stage I), then dislocation clusters (stage II), and then dislocation cells (stage III).

A completely different mechanism of strain hardening is observed during dynamic tests with compression rates within the range $1250-1390 \, \mathrm{s}^{-1}$ (Fig. 10, c). In this case, the strain hardening of the homogeneous deformation stage is well described by the single exponent n=1. This means that compression deformation is controlled exclusively by dislocations shear overcoming of the α -plate. It can be assumed that dislocations pass through some substructure formed in α -plates during the dynamic relaxa-

tion of high elastic stresses. Most likely, it is something similar to a cellular substructure without any misorientations. However, this assumption needs serious experimental confirmation, which has not been done yet.

However, the most interesting thing happens with a seemingly insignificant increase in the strain rate by about 1000 s⁻¹ (up to 2230 s⁻¹; Fig. 10, d), when the strain hardening mechanism changes dramatically. The values of the n exponent range from 0.6 to 0.9, which indicates the equal probability of α -plates and β -layers acting as phases controlling strain hardening. It should be noted here that n in the case of an alloy with an LM structure does not reach the limiting values of 0.5 and 1.0, which are characteristic of the twin-controlled mechanism described above for the same material with a globular microstructure. This is evidence that, in the case of flat interphase surfaces, no local stress concentration occurs on them under dynamic compression, and stresses relax by interphase slip. Most likely, such local stress concentrations will occur on curved surfaces, such as the boundaries between α - and β -phases in a globular microstructure. This is probably possible when the process is controlled by interphase boundaries, where dislocations respond equally well to thin α - and β -layers of nanometer thickness. In other words, in this situation, it can be argued that there is a certain limiting rate of deformation, at which there is a transition from the mechanism of strain hardening controlled by the bulk phase (α) to the mechanism controlled by the interphase α/β -boundary. Available facts indicate that the mechanism of slippage along the interphase boundaries is currently implemented.

2.3.3. Ti64 with Lamellar Initial Microstructure Manufactured Using Blended Elemental Powder Metallurgy Approach (Ti64BEMP)

In general, the microstructure of the Ti64BEPM alloy (blending elements powder metallurgy) is lamellar, similarly to the structure of the Ti64LM alloy, with the difference that the alloy obtained by the powder metallurgy method has smaller β -grains' size (not more than 100 μ m vs above 500 μ m in Ti64LM material), and some amount of pores (about 2%; Fig. 11).

At first glance, the stress-strain curves for a given structural state (Fig. 12, a) are an intermediate option between the globular (Fig. 8, a) and coarse lamellar (Fig. 10, a) structures, primarily in terms of plastic properties. Obviously, these are the features of the microstructure, which, in a certain way, affect the mechanical behaviour of the material and influence the strain hardening of the alloy under compression. Thus, in case of quasi-static compression, only one initial stage of strengthening with the most probable indicator n = 0.7 is found (Fig. 12, b). The rest of the curve is not described by the usual strain hardening and is not divided into a series of rectilinear sections for any values of n. Nevertheless, the value of n = 0.7 may indicate that, in this case, the deformation mechanism at the initial stage of deformation is equally controlled by both

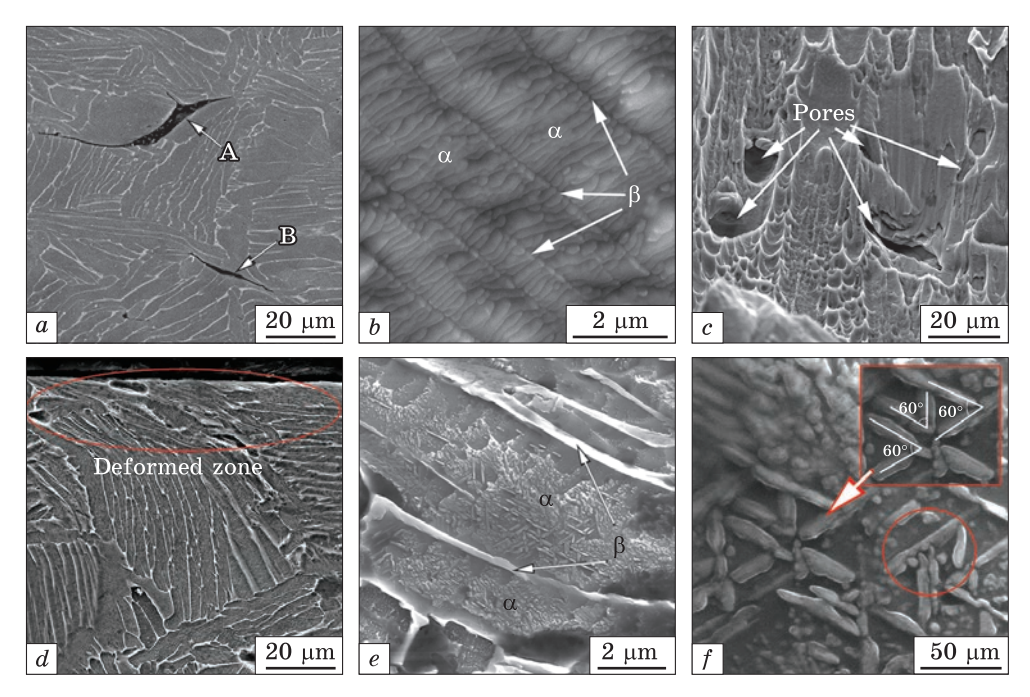


Fig. 11. SEM images of the fracture surface of the Ti64BEPM alloy tested at strain rates of 10^{-3} s⁻¹ (a, b) and 2220 s⁻¹ (c-f): c — zone I; d — zone II; e, f — zone IV in Fig. 7, a [31]

α-plates and β-layers. We have already noted above that this situation most likely occurs when the strengthening mechanism is controlled by interphase boundaries. At the next stages of uniform deformation, a substructure of 200-300 nm in size is formed within α-plates and β-layers (Fig. 11, b). It can be assumed that a substructure of this type does not obey the power law of strain hardening under quasi-static compression. This is what is reflected in the curves (Fig. 12, b), when trying to process them using Eq. (1). It is also impossible to exclude a certain influence of pores as some third phase having specific properties, which are difficult to take into account.

The transition to dynamic tests of the Ti64BEPM alloy changes the situation with strain hardening. Thus, in the range of dynamic compression rates of $1600-2220~{\rm s}^{-1}$, hardening at a homogeneous stage of deformation is characterized by a hardening exponent of n=1 for all rates, and is described by two coefficients of deformation hardening which differ weakly each other (Fig. 12, c). This may indicate that, firstly, strain hardening is controlled exclusively by α -plates, and secondly, the entire stage is practically characterized by one type of substructure in these plates. The type of substructure inside α -plates is needles of the martensite type [31] (Fig. 11, e, f). That is, strain hardening at dynamic compression rates

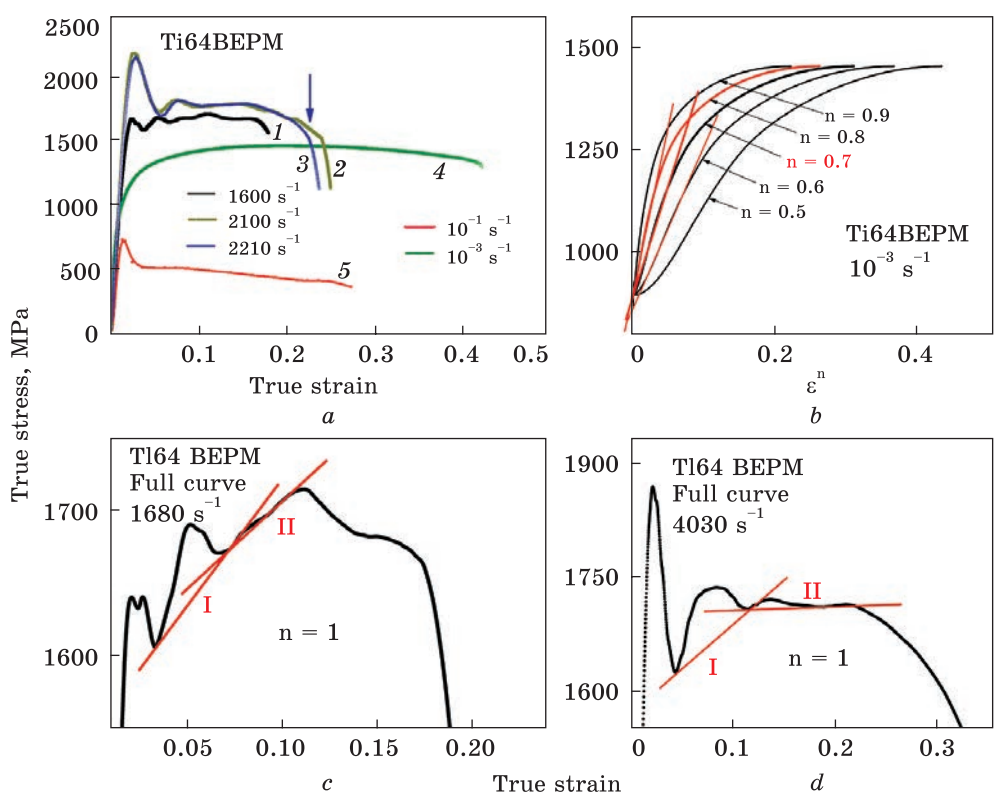


Fig. 12. Analysis of homogeneous sections of the compression curves of the Ti64BEPM alloy deformed at different rates: a — original curves in coordinates true stress—true strain [31]; b — the result of representing the quasi-static compression curve; c — the result of the same presentation of dynamic compression curves with different strain rates

of $1600-2220~s^{-1}$ is determined by martensite needles distributed inside α -plates. It was shown in Ref. [31] that martensite needles of submicroscopic size can be formed during rapid heating associated with high deformation velocity and subsequent cooling. It should be noted that there is no direct connection between the presence of residual pores and the formation of martensite. The collapse of pores during very rapid deformation may cause the formation of local high stress gradients, which can contribute to the nucleation of martensite needles.

The transition to a higher level of dynamic compression (3170–4030 s⁻¹) does not change the mechanism that controls strain hardening with an index of n=1. However, this strain rate level is characterized by two clearly seen stages of the strengthening coefficient (Fig. 12, d). Moreover, as can be seen in Fig. 12, d, no strengthening occurs at the second stage of strain hardening. In the absence of microscopic data, it is difficult to judge what type of substructure controls second-stage strength-

ening. One can only speculate that if the first stage is controlled by martensite needles, then perhaps a secondary α -phase is formed in the second stage, which may be facilitated by a high rate of strain and, accordingly, a higher level of unrelaxed mechanical stresses. However, this assumption has not been confirmed.

2.4. Metal Matrix Composites Reinforced with TiB and TiC Particles

These metal matrix composites (MMC) reinforced with hard particles were prepared using the BEPM approach with some specific modifications [34, 45, 46]. Such a metal matrix composite is a three-phase compound consisting of α -, β -, and TiC or TiB phases, and was designed for the improvement of some characteristics, like average hardness, wear resistance, etc. Such a metal matrix composite is a three-phase compound consisting of α -, β -, and TiC or TiB phases, and was designed for the improvement of some characteristics, like average hardness, wear resistance, etc.

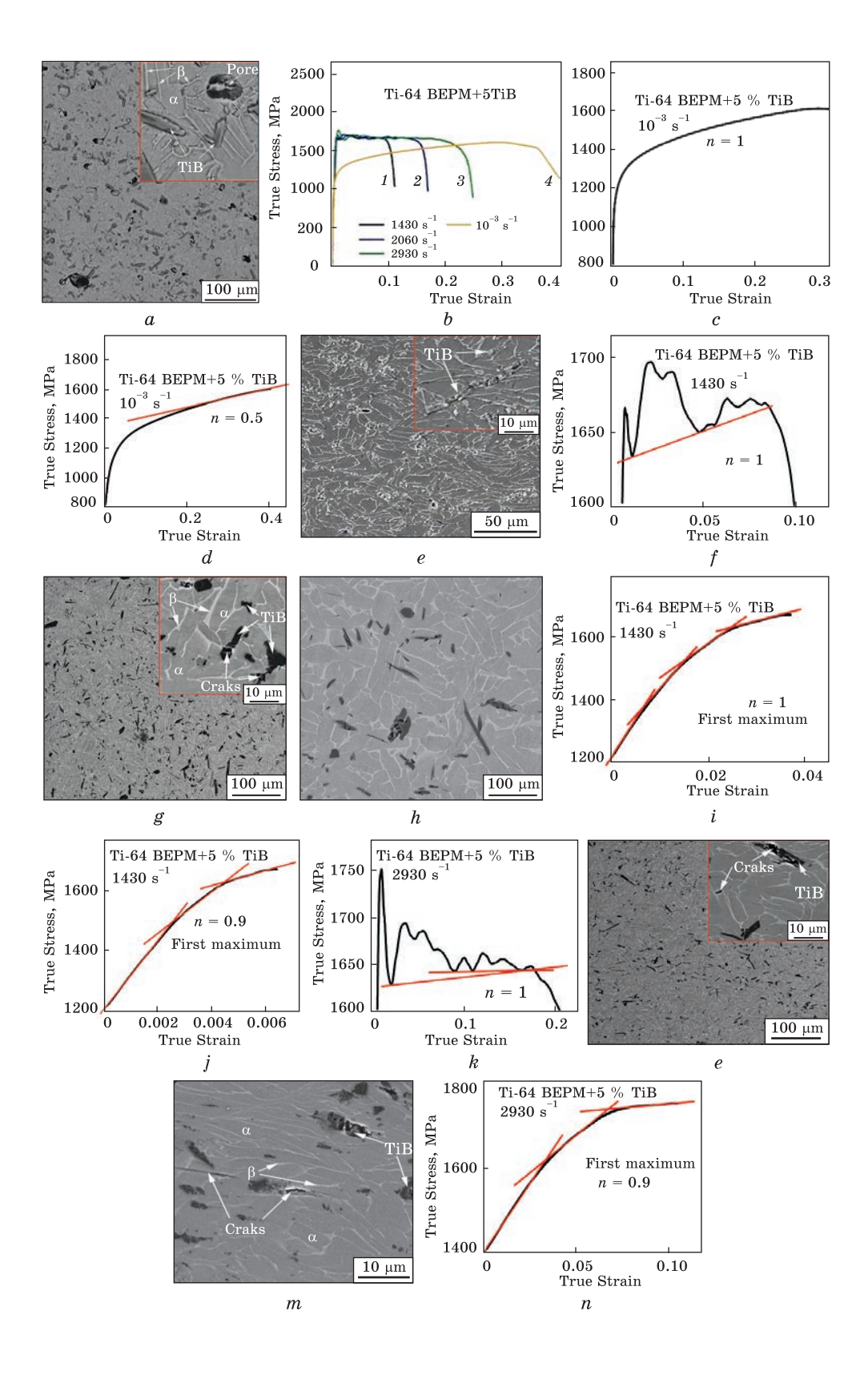
2.4.1. Ti64BEPM + xTiB

2.4.1.1. Ti64BEPM + 5%TiB

The initial microstructure of metal-matrix composites (MMC) with micron-sized TiB solid particles based on the Ti–6Al–4V alloy, also manufactured by blended elemental powder metallurgy (BEPM), is shown in Fig. 13, a. The matrix structure is a conventional lamellar structure consisting of alternating α -plates and β -layers. Most of the TiB particles have the character of short, elongated bars or needles with a length varying from 5 to 50 μm . Being sufficiently uniformly distributed in the volume of the titanium matrix, these particles have a pinning effect that restricts the growth of matrix β -grains. The surface of the particles looks quite smooth, at least at the magnification presented. In addition, a sufficiently large number of pores with an average size of 10–20 μm are observed in the structure.

True stress—true strain curves of quasi-static and dynamic compression of MMC Ti-6Al-4V material with 5% TiB particles (Ti64 + 5% TiB) are presented in Fig. 13, b. The material subjected to a quasi-static compression at a strain rate of 10^{-3} s⁻¹ has a pronounced character of strain

Fig. 13. Microstructure (SEM) and compression curves of Ti64BEPM + 5% TiB alloy: a-e — quasi-static compression; a — initial structure after synthesis from elemental powders and TiB powders (sintering); b — deformation curves after synthesis; c — quasi-static compression curve; d — processing of this curve according to Eq. (1) with n = 0.5; e — microstructure after quasi-static compression; f — dynamic compression curve at $1430 \, \mathrm{s}^{-1}$; g, h — microstructure after dynamic compression at this strain rate; i, j — representation of the first maximum of the dynamic compression curve compression at a strain rate of $1430 \, \mathrm{s}^{-1}$; k — dynamic compression at this strain rate; representation of the first maximum of the dynamic compression at this strain rate; representation of the first maximum of the dynamic compression curve with a strain rate of $2930 \, \mathrm{s}^{-1}$ [34]



hardening. However, the strain hardening effect has an unusual appearance. The transformation of the compression curve using Eq. (1) and a hardening index n = 1 (Fig. 13, c) shows that only with a hardening index of n = 0.5 (Fig. 13, d) can at least part of the uniform deformation curve be brought closer to a form suitable for qualitative analysis. So, only the final part of the curve can be approximately described using the smallest possible hardening index n = 0.5. That is, it is likely that in the end, in the presence of reinforcing particles, the work hardening is controlled by β-layers. The microstructure changed significantly after the test: the lamellas became distorted, the TiB particles became much smaller, and the pores became an order of magnitude smaller (Fig. 13, e). Such a structure transformation should have been reflected in the deformation curve. Initially, the hardening under quasi-static compression of Ti64BEPM + 5% TiB does not obey the exponential law. It can be assumed that, at the initial stages of compression, TiB particles effectively prevent the slip of dislocations, and the density of dislocations around them increases. Then, when the limiting density of dislocations is reached, further hardening is ensured by overcoming the accumulated dislocations of the β-layers very close to the TiB particles. Figure 13, f indirectly confirms the stated assumption. On the other hand, intensive pores collapse took place simultaneously, which probably, in principle, cannot be described by an exponential dependence of stress on strain. Perhaps this is due to the competition between the change in volume energy with a decrease in the pore volume and the surface energy with a reduction of the free surface of pores.

The dynamic compression curves at different strain rates are almost the same (Fig. 13, b). Moreover, in this representation, it is not clear whether they express hardening in the process of deformation or softening since the resolution of the curves in Fig. 11, b is not enough. Figure 13, f shows the deformation curve of the Ti64BEPM + 5% TiB alloy at a rate of 1430 s⁻¹. Unfortunately, this curve represents oscillatory changes in stresses with strain; the location of the minima does not obey the law (1) and does not decompose into straight sections for any values of the exponent n. Therefore, the first thing that could be done was to determine the general trend, whether the material is strengthened or weakened in the process of deformation. To do this, it is necessary to designate the lowest values of two of all minima on the curve and connect them with a straight line, as is done in Fig. 13, f. The minima are taken because they represent the values of stress relaxation during deformation. Since the straight line in Fig. 13, e ascends, this means that the Ti64BEPM + 5% TiB alloy under compressive deformation at the strain rate of 1430 s⁻¹ is generally hardened. Since this is not enough to determine the strain hardening mechanism, it was proposed to analyse the hardening curve of the first maximum of the general curve using the general scheme of Eq. (1). The result is shown in Fig. 13, i, j. From this Figure, the best approximation is obtained at n = 0.9. This means that with a very rapid increase in strength, the dislocations do not sense the hard TiB particles, and the hardening is determined purely by the plates of the α -phase. The presence of three rectilinear sections on the transformed hardening curve means that in the case of superfast hardening, the microstructure undergoes a classical transformation from a chaotic distribution through coils and tangles to a cellular substructure. Comparison of strain hardening curves under quasistatic and dynamic compression of BEPM alloys without hardening particles (Fig. 12) with curves for similar alloys with TiB particles (Fig. 13) shows that the presence of particles does not give a significant gain in either strength or ductility of the material. As will be shown below, the presence of particles has a significant effect on the softening of alloys during quasi-static and dynamic compression.

As already noted in Ref. [34], no significant evidence of plastic deformation in the $\alpha + \beta$ -matrix, studied using SEM, is observed under dynamic compression of the alloy with 5% TiB. The only signs of deformation of MMC as a whole were cracks in the TiB particles (Fig. 13, h). At the same time, the appearance of such cracks is a sign of stress relaxation. On the other hand, the compression curve (Fig. 13, e) indicates that the alloy (matrix) hardens during compression. The only way to eliminate this contradiction is for stress relaxation by cracking TiB particles occurs with a relatively small number of particles. Most of the particles fulfil their strengthening function. This is seen in Fig. 13, h, where the bigger TiB particles did not undergo cracking.

Increasing the strain rate to 2930 s⁻¹ (Fig. 13, k) results in negligible hardening throughout the compression process with a slightly lower hardening rate if the first minimum is taken as the starting point. If we do not take into account the first minimum, then the remaining three minima fit well on a straight line, almost parallel to the x-axis. This means there is no strain hardening effect. The reason for this is the significantly larger number of particles that break under high-speed compression (Fig. 13, l, m) compared to the lower strain rate loading (Fig. 13, g).

2.4.1.2. Ti64BEPM + 10%TIB

Doubling the content of TiB reinforcing particles in the Ti64BEPM matrix to the level of 10% (Fig. 14, a) at first glance does not change the nature of the quasi-static and dynamic compression of the alloy (Fig. 14, b). However, an in-depth analysis of the results suggests otherwise. The processing of the quasi-static compression curve (Fig. 14, c) according to Eq. (1) (Fig. 14, d) shows that the best result is obtained when the hardening index n = 0.5. At the same time, only the initial and final sections of the quasi-static compression curve are subject to the representation with such a hardening indicator (Fig. 14, d). The middle portion of the curve is purely non-linear. The value n = 0.5 reflects the fact that in the first and

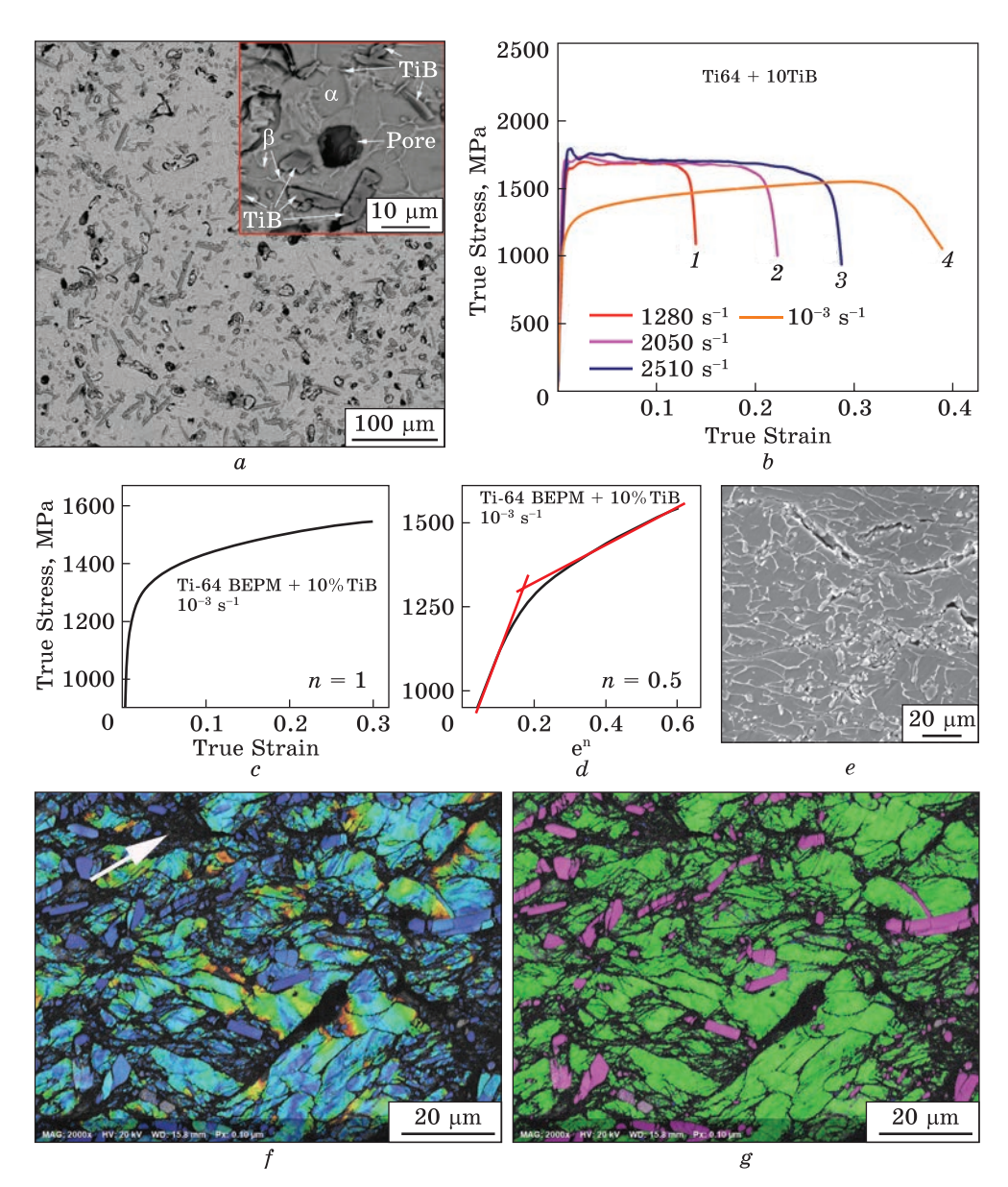
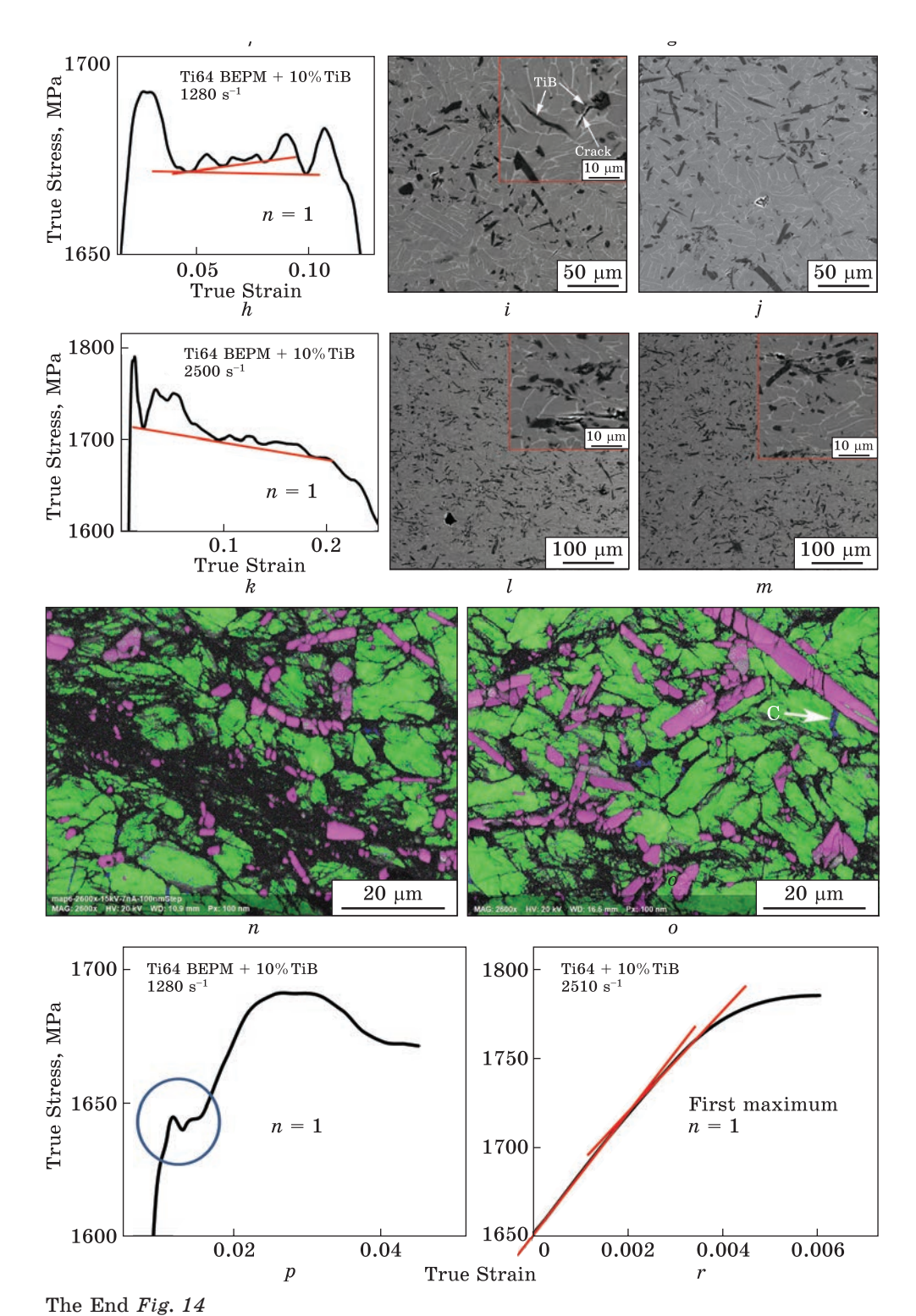


Fig. 14. Microstructure (SEM and EBSD) and compressive strain curves of Ti64BEPM + + 10% TiB alloy: a-g — quasi-static compression; a—initial structure after synthesis from elemental powders and TiB powders (sintering); b — deformation curves after synthesis; c — quasi-static compression curve; d — processing of this curve according to Eq. (1) with n = 0.5; e — microstructure after quasi-static compression; f — distribution map of intergranular misorientations; g — phase distribution map after quasi-static compression (colour online, green — α -phase, blue — β -phase, magenta — TiB particles); h — dynamic compression curve at 1280 s⁻¹; i, j — microstructure after dynamic compression at this strain rate; k — dynamic compression curve at 2510 s⁻¹; l, m — microstructure after dynamic compression at this strain rate of 1280 s⁻¹; o — processing the first maximum of the compression curve at a strain rate of 2510 s⁻¹ according to Eq. (1); p, r — distribution of phases after compression at a strain rate of 2510 s⁻¹; p — in the region of the adiabatic compression band in zone II; r — near zone III in Fig. 7, a [34, 36]



ISSN 1608-1021. Usp. Fiz. Met., 2025, Vol. 26, No. 3

last sections of homogeneous compression, the deformation is controlled by a phase whose crystal lattice differs significantly from the h.c.p. lattice. In the first section, most likely, this is the β -phase, the interlayers of which are visible in Fig. 14, g in the form of thin strips about 1 µm thick adjoining the reinforcing TiB particles. The tight connection of the interlayers of the β -phase with solid TiB particles creates conditions for the relatively soft β-phase to serve as an obstacle to its complete overcoming by the rapidly increasing dislocation density at the first stages of compression. Then, when the dislocations reach the boundary between the β-phase and the TiB particle, the β-phase becomes a factor that does not control the deformation. Now, there comes a period when, at the boundary between the β-phase and the TiB particle, the density of dislocations with compressive strain increases to a certain limiting value. This period is described by the nonlinear part of the curve. When the density limit value is reached, a period of formation in the α -matrix near the TiB particles of a cellular substructure begins, which is seen in Fig. 14, f, g. Taking into account the straightness of the final section with n=0.5 and the described course of events, it can be assumed that the deformation mechanism at this stage is controlled by TiB particles. In other words, n = 0.5 does not necessarily mean that the mechanism-controlling phase is the β -phase. Probably, such a phase can also be a TiB particle, which has an orthorhombic lattice [45].

The curve of dynamic compression of the Ti64BEPM + 10% TiB alloy at a strain rate of $1280 \, \mathrm{s}^{-1}$ is shown in Fig. 14, h. This curve, as well as for the case with 5% TiB (Fig. 13, f), represents oscillatory changes in stresses with deformation; the location of the minima does not obey the law (1) and does not decompose into straight sections for any values of the exponent n. Its processing has shown that the mechanical behaviour of the alloy containing 10% TiB is fundamentally different from the behaviour of the alloy containing 5% TiB. Namely, in contrast to the 5% TiB alloy, which exhibits stable hardening at $1430 \, \mathrm{s}^{-1}$, the $10\% \, \mathrm{TiB}$ alloy experiences slight softening during compression, bordering on no softening (Fig. 14, h). Analysis of the microstructure (Fig. 14, h), shows that there are no significant changes compared to the initial state (Fig. 14, h), except for the appearance of small cracks, although it is most likely that these cracks appear at the end of the deformation. The process of slight softening may be associated with rare cracks that are observed on TiB particles (Fig. 12, h, h).

Increasing the compression rate to 2510 s^{-1} (Fig. 14, k) leads to more significant softening throughout the compression process with a higher softening rate. The nature of this difference in the behaviour of the material during deformation is that an increase in the compression rate contributes to the significant refinement of the TiB reinforcing particles, which occurs as a result of their cracking (compare Fig. 14, i and j with l and m). The fact that the particles are cracking is evidenced by the results of the phase analysis presented in Fig. 14, n, o.

As in the case of the Ti64BEPM + 5% TiB alloy, the analysis carried out above on the full curve is not able to determine the features of the hardening mechanism at the stage of uniform deformation under dynamic compression. It was proposed to analyse the hardening curve of the first maximum of the general curve according to the general scheme of Eq. (1). The results for the two strain rate levels are shown in Fig. 14, p, r. It can be seen from the figure that for a lower strain rate of 1280 s⁻¹, it is not possible to expand the first maximum at all, since it is not described by a smooth curve, but is an analogue of a low-yield tooth (indicated by an oval in Fig. 14, p). As the dynamic compression rate increases to 2510 s^{-1} , the yield tooth turns into a sharp first maximum (Fig. 14, k). The expansion of this maximum according to Eq. (1) leads to two straight sections with n=1, and the last section of the curve is not described by law (1). This means that, as in the case of compression of the alloy with 5% TiB, the strain hardening of the Ti64BEPM + 10% TiB alloy at the earliest stages (the first two sections of the first maximum) is controlled by the processes of slip and dislocation accumulation occurring in the α -phase. At the last stage of the first maximum, TiB particles are probably included in the process. The result obtained indicates that an increase in the content of TiB reinforcing particles in the alloy leads to an increase in the efficiency of composite matrix hardening.

2.4.2 Ti64BEPM + xTiC

First, we will analyse the influence of strengthening TiC particles on the mechanism of the strain hardening of MMCs based on the BEMP Ti-6Al-4V (Ti64) alloy under quasi-static compressive loading conditions. Figure 15 shows the stages of homogeneous deformation of the hardening curves treated according to Eq. (1) with different contents of TiC particles and their corresponding microstructures before and after deformation at a strain rate of 10^{-3} s⁻¹.

First of all, it should be noted that both before (Fig. 15, a, e, i) and after compression, TiC particles are distributed inhomogeneously over the volume, forming conglomerates of different densities. This is probably a manifestation of thermodynamic features of the interaction of micronsize TiC particles with the Ti64 matrix. It is also necessary to take into account the presence of residual pores, which can influence a significant variation in particle sizes (10–50 µm). The curves of hardening under quasi-static compression for alloys with different contents of TiC particles at the stage of homogeneous deformation are most adequately described by the strengthening index n = 0.5 (Fig. 15, b, f, j). In turn, these curves are described not completely but only in the first two sections. The last section is not in accordance with the usual exponential law, even if it is approximated by values n = 0.1-0.4, *i.e.*, it is characterized by significant nonlinearity. The reason for this, most likely, is in the specific nature

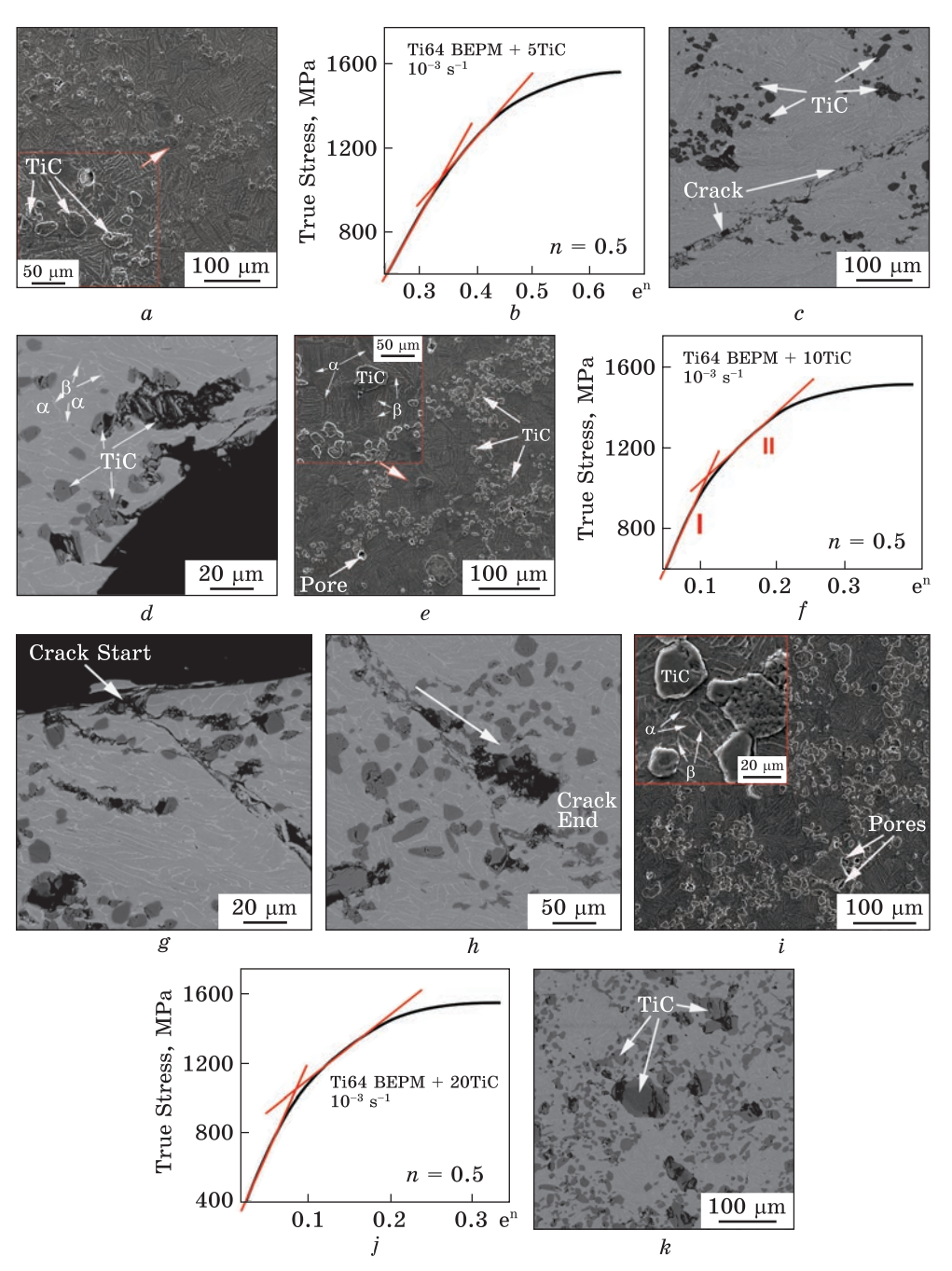


Fig. 15. SEM-BSE microstructure of MMC alloys before testing for quasi-static compression with different contents of TiC particles, 5% (a), 10% (e), 20% (i), corresponding strain hardening curves under quasi-static compression at a strain rate of 10^{-3} s⁻¹ (b, f, j) presented as Eq. (1) as well as SEM-BSE microstructure after compression (TiC content 5% (c, d), 10% (g, h), 20% (k)) [34]

of the structure change during compression associated with the presence of pores.

The initial microstructure before compression is shown in Fig. 15, a, e, i. Careful analysis shows that at any content of TiC particles, they are surrounded by a layer of β -phase. It is this β -phase, according to the value of n = 0.5, which controls the mechanism of strengthening in the first two areas of deformation and microstructure formation. At first, as usual in alloys with a lamellar structure, dislocations slide before meeting with particles of TiC. Since these particles are surrounded by the β -phase, this phase plays the role of the factor controlling strengthening. Dislocations accumulating on the boundary between the β -phase and the particle and in the β -phase itself form clusters and intertwine at further deformation, as evidenced by the presence of the second rectilinear section at n=0.5. However, this law of linearity is further violated with increasing strain. The reason for this is that under the action of high compressive stresses and with the assistance of accumulated dislocations, the β-phase is dissolved along the dislocation core by the corresponding diffusion mechanism. This occurs almost at room temperature since the strain rate is not so high that the material heats up strongly.

The fact that the β -phase resorbs is evidenced by the SEM BSE data performed after deformation (Fig. 15, c, d, g, h, k). It can be seen that the TiC particles are not surrounded by the β -phase and the particle boundaries are less clear than before compression. In addition, large particles show a central, darker zone and a peripheral, lighter zone (Fig. 15, k). This means that there is more carbon in the darker zone, and hence, there is diffusion of carbon during compression, and some small amount of carbon may be transferred into the alloy matrix. Thus, in the process of quasi-static compression of MMC based on BEPM Ti-6Al-4V (Ti64) alloy with TiC particles, the β -phase surrounding TiC particles and controlling strengthening at the beginning of homogeneous deformation, dissolves in the matrix in the course of deformation. Further strain hardening is controlled by TiC particles by the mechanism of dispersion hardening.

Next, we perform a general analysis of the dynamic compression curves of MMC with micron-sized TiC particles (Fig. 16). First of all, the similarity of deformation curves under dynamic compression attracts attention (Fig. 16, a) for alloys with different content of TiC particles but tested at almost the same strain rates (except for the alloy without TiC). It is the identity of the alternation and similarity of the positions of maxima and minima of the hardening curves. Moreover, if we rearrange these curves according to Eq. (1), this identity is even clearer (Fig. 16, b-i) both for alloys with different content of TiC particles and for different compression rates. The most surprising thing is that the identity of the curves depends weakly on whether there are TiC particles in BEPM alloy Ti-6Al-4V or not.

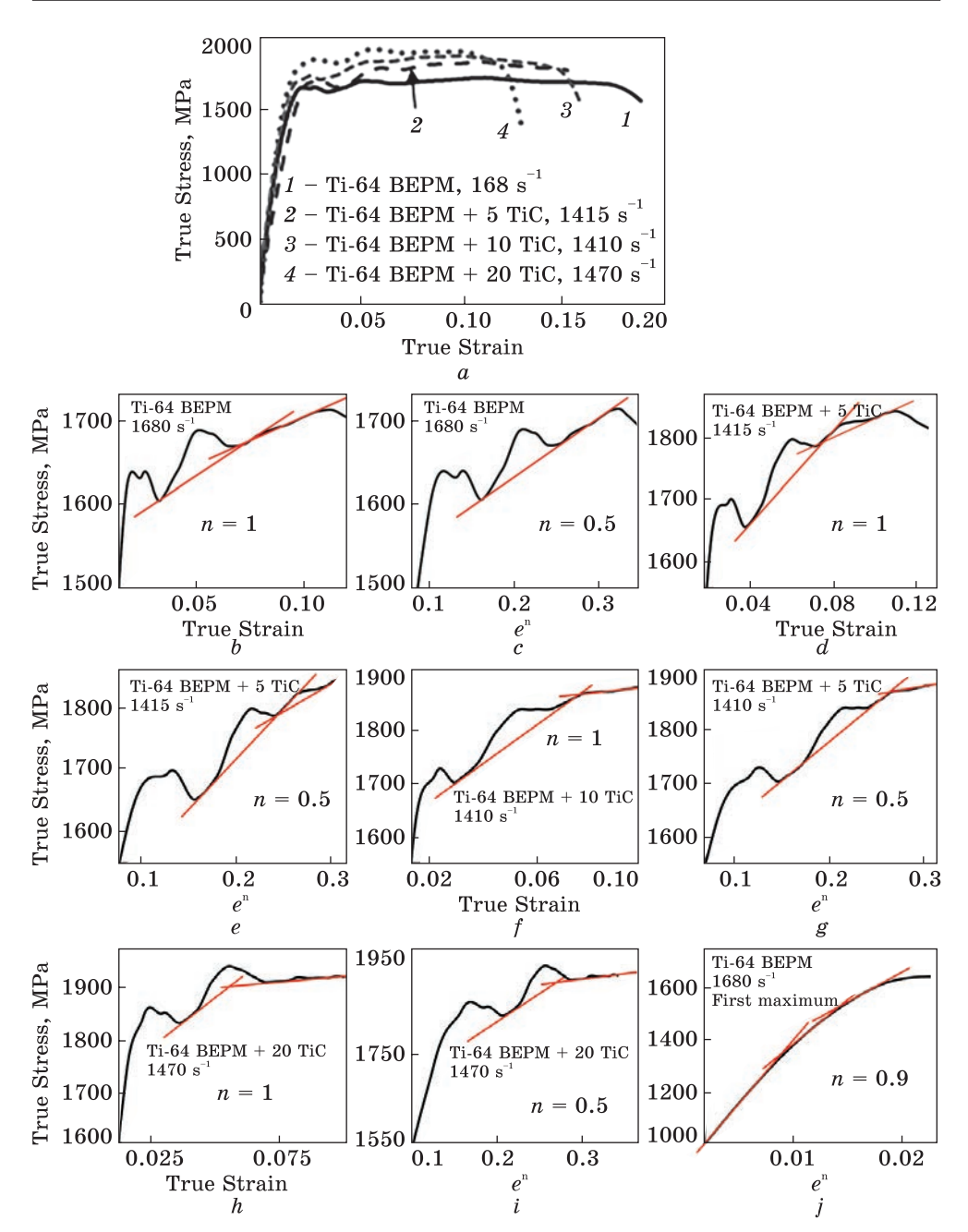
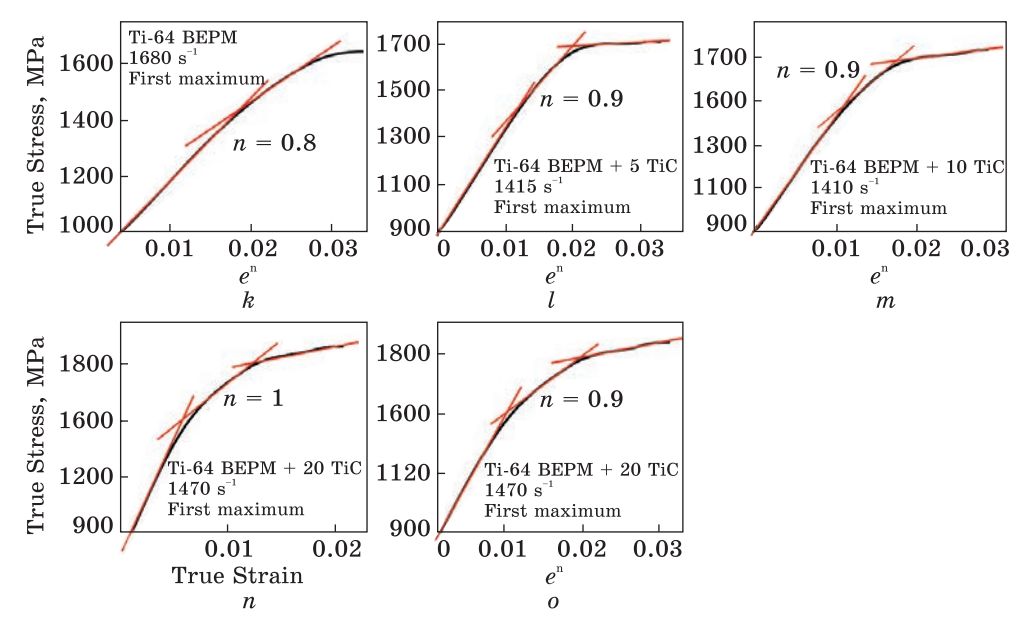


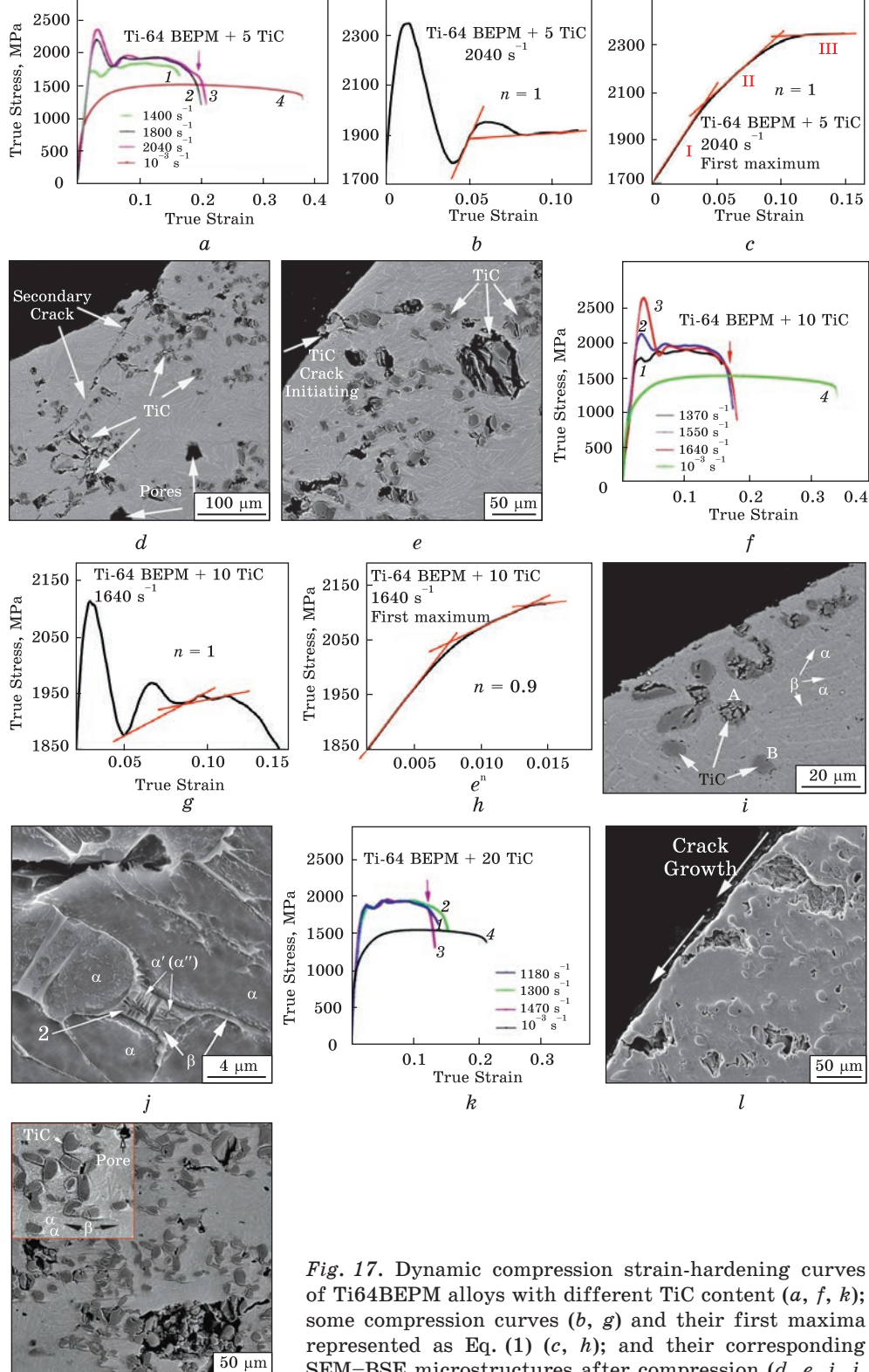
Fig. 16. Hardening curves under dynamic compression of Ti64 alloy (Ti64BEPM state) and MMC on its base hardened with different content of TiC. General view of curves with different content of hardening TiC particles (a), and curve analysis by Eq. (1): general analysis of the alloy curve without TiC (b, c), with 5% TiC (d, e), with 10% TiC (f, g), with 20% TiC (h, i); analysis of the first maximum of the alloy curve without TiC (j, k), with 5% TiC (l), with 10% TiC (m), with 20% TiC (n, o) [34]



The End Fig. 16

Indeed, if we compare the dynamic compression curves of Fig. 16 b, c with the rest of the curves of the same Fig. 16, we can see that all states are, to some extent, equally well described by the strengthening indices of both n=1 and 0.5. As has been shown above for other Ti64-based alloys, this fact indicates that in this case, the dynamic compression strengthening mechanism is controlled by both α - and β -phases simultaneously. This is possible in a lamellar structure only when the compressive strain is controlled by slip along the α/β -interphases. The role of strengthening TiC particles is reduced here to limiting this slip, *i.e.*, inhibiting the slip of dislocations along the α/β -interphase boundaries, which extend to the boundaries of TiC particles. In other words, the limitation of slip along interphase boundaries, in this case, plays a more important role than the inhibition of dislocations sliding in their slip plane.

For almost all TiC contents and strain rate levels, two hardening sections are observed at the stage of homogeneous deformation. This indicates that strengthening is associated with two stages of microstructure development. The first one is probably related to the accumulation of dislocations in the interphase boundaries in the form of dislocation clusters, and the second one is caused by the rearrangement of these clusters into dislocation cells with non-misoriented boundaries. In this connection, it is important to note that in the above strengthening mechanism, the primary section associated with the accumulation of chaotically distributed dislocations, which is characteristic of the most previously considered cases of compression of titanium alloy Ti64, is most likely impossible.



m

SEM-BSE microstructures after compression (d, e, i, j,l, m) [34]

The approximation of the homogeneous stage of the curve by Eq. (1) for the alloy without TiC at n=0.5, which is represented by only one straight line (Fig. 16, c), deviates from the general picture. This may mean that in the case of the alloy without TiC particles, the controlling process of strain strengthening in the interphase boundary is more related to the β -phase. There is no explanation for this fact yet. Maybe, in this case, when there are no strengthening particles, the influence of pores is affected.

Since there is practically no microstructural data for the curves presented in Fig. 16, we analyse the results for the first maxima using Eq. (1) for additional information. The approximation results are presented in Fig. 16, j-o. It should be noted that for almost all cases, the first maxima of the dynamic compression curves are described by the hardening index n=1 or close to it. It seems that, at very high hardening rates during dynamic compression, either dislocations do not feel the β-phase, which surrounds TiC particles, or the β -phase is quickly destroyed. In this case, the deformation mechanism is controlled either by the α -phase or by the TiC particles, whose crystal structure is an octahedral lattice [14]. It is clear that in the absence of β-phase surrounding TiC particles; only these particles can be an effective strengthening element. Note that all alloys with TiC exhibit three classical areas of microstructure formation (Fig. 16, l-o) at a high strain rate of strengthening growth, which consistently characterizes the accumulation of chaotically distributed dislocations, the formation of dislocation thickenings, interweavings, and the formation of non-misoriented dislocation cells. On the other hand, the alloy without TiC shows only first two straight-line sections; the remaining section is not described by the law (1). In this section, where there is a complete damping of strengthening at the first maximum, such rearrangements of the structure likely occur, which are yet to be revealed.

The deformation curves of Ti64BEPM alloys with 5% of TiC (Fig. 17, a) and with 10% of TiC (Fig. 17, f) tested at high strain rates are characterized by the presence of high first maxima. Analysis of these curves (both the full curves and their first maxima) by Eq. (1) allows us to conclude that strain hardening is described by an exponent n equal to or close to 1. This means that both at the high rate of strengthening growth at the first maximum and deformation at the rest stage of homogeneous deformation, dislocations do not feel the influence of either TiC particles or the β-phase interlayer surrounding these particles. The latter is evidenced by the presence of the β -phase interlayer partially located in the vicinity of the TiC particles (Fig. 17, e, l, m). Hence, it can be concluded that the β -phase can influence the deformation mechanism only when it completely surrounds the TiC particles, where there are no areas of contact between the particle and the α -phase. Since strengthening is characterized by the degree n=1, it is natural to conclude that the influence of TiC particles on the deformation mechanism is also described by exponent n=1, as well as the α -phase. This means that there is no sharp boundary between the TiC particles and the surrounding α -phase, and the crystal lattice of the particle seems to grow into the crystal lattice of the α -phase. This is evidenced by the data in Fig. 17, i, l. That is, these structures are in a certain sense conjugated. This does not mean that the particles in this case do not have a strengthening effect. Dislocations slide freely in the α -phase and then penetrate TiC particles, where they experience inhibition (the lattice is different after all), and their velocity becomes significantly lower. At the same time, the interaction between dislocations increases; they accumulate and create conditions for the formation of cracks inside the particles, which is visible in almost all the structures shown in Fig. 17.

The strain curves for the case of Ti64BEPM + 20% TiC rearranged by Eq. (1) are presented in Fig. 17, h, i, n-p. As seen, in the case of not very high strain rates (1470 s⁻¹) but high concentration of TiC particles, the strengthening for the first maximum is equally well described by both n=0.5 and n=1. For the full curve, the hardening index is close to n=1. Based on the above reasoning, we can conclude that there is a certain limiting velocity of dynamic compression, above which the β -phase surrounding the TiC particles either dissolves or collapses during compression. After that, the α -phase controls the dynamic compression mechanism.

2.4.3. Influence of the Pores

Pores in some quantities are always present in materials synthesized by powder metallurgy methods [46–48]. With a certain assumption, they can be considered as some additional phase, which, in quantities exceeding 1.5–2%, significantly reduces the mechanical properties of the synthesized material in tensile and fatigue tests, serving as centres of crack initiation. However, during compression tests, the pores do not have a negative effect, since they are flattened and disappear [34]. On the contrary, if the number of pores increases to such an extent that such material already belongs to the category of highly porous, then under conditions of quasistatic and dynamic compression, it becomes an effective absorber of the applied energy [49–51].

2.5. High-Alloyed α + β Ti-5.5(wt.)% Al-1.5V-1.5Mo-4Nb-2.0Fe-0.7Zr (T110) Alloy

Among all the titanium alloys studied for the regularities of their behaviour (see also Refs. [52–55]), the evolution of the microstructure, and the determination of the phases that control strain strengthening under quasistatic and dynamic compression, the T110 alloy occupies a special place. First of all, because it was tested after a series of successive treatments: annealing after casting, 3D-pressing in the β -region, deformation by rolling below the temperature T β and subsequent heat treatment, which stabi-

lized the phase composition and microstructure (annealing at 850 °C for 3 h, followed by cooling with a furnace). What is important to underline, the microstructure of the T110 alloy in this state is characterized by a mixed type, consisting equally of equiaxed and elongated α -phase particles (Fig. 18, a), surrounded by approximately half of the volume by β -phase interlayers, which are also elongated along the rolling direction (Fig. 18, b). These layers are interspersed with equiaxed sections of the \beta-phase. Approximate phase ratio $\alpha/\beta = 70:30$ (Fig. 18, b). In addition, the structure is characterized by some amount of secondary α-phase of nanoscale thickness, which has precipitated inside of β -phase (Fig. 18, b, inserted in the top right corner). This type of microstructure leads to high strength and especially high plasticity under quasi-static compression, especially if the compression direction coincides with the rolling direction (Fig. 18, c). Reconstruction of the strengthening curves in the σ - e^n co-ordinates (Fig. 18, d) shows that the homogeneous stage of deformation is described by the exponent n = 0.7. This means that neither the α - nor the β -phase individually controls the deformation/strengthening mechanism of the T110 alloy in the annealed state after rolling. Since the direction of compression coincides with most of the interphase boundaries, this behaviour is most likely related to the deformation mechanism controlled by sliding along the phase boundaries, when the influence of both α - and β -phase is equally likely to be manifested. This is facilitated by the large misorientation angles between the α - and β -phases, as can be seen from the scattered texture patterns for samples rolled to a thickness of 15 mm [32]. At such misorientation angles, the transfer of dislocation slip from one phase to another is significantly difficult. Along with the secondary α -phase, this is an important component of the high strength of the alloy. Dislocations are inhibited at the interphase boundaries and form centres of stress, which subsequently relax by sliding along the interphase boundaries. Such a microstructure (in the annealed state after casting and after 3D-pressing in the β -region) ensures extremely high plasticity of the alloy (almost 0.7) under quasi-static compression in the rolling direction.

A comparison of the obtained results with the microstructural features of the different locations in the sample deformed by quasi-static compression in the annealed state along the rolling direction allows us to conclude the following. The most likely part of the microstructure of the sample, which is responsible for the mechanism that controls strain hardening during quasi-static compression, is the microstructure of the section identified by the letter A in Fig. 18, e. In this area, the interphase boundaries are stretched vertically in the direction of action of the applied load, which corresponds to the direction of sliding along the interphase boundaries. It should be noted that, according to Fig. 18, e, most of the volume of the sample deformed by compression is similar to section e in terms of microstructure features.

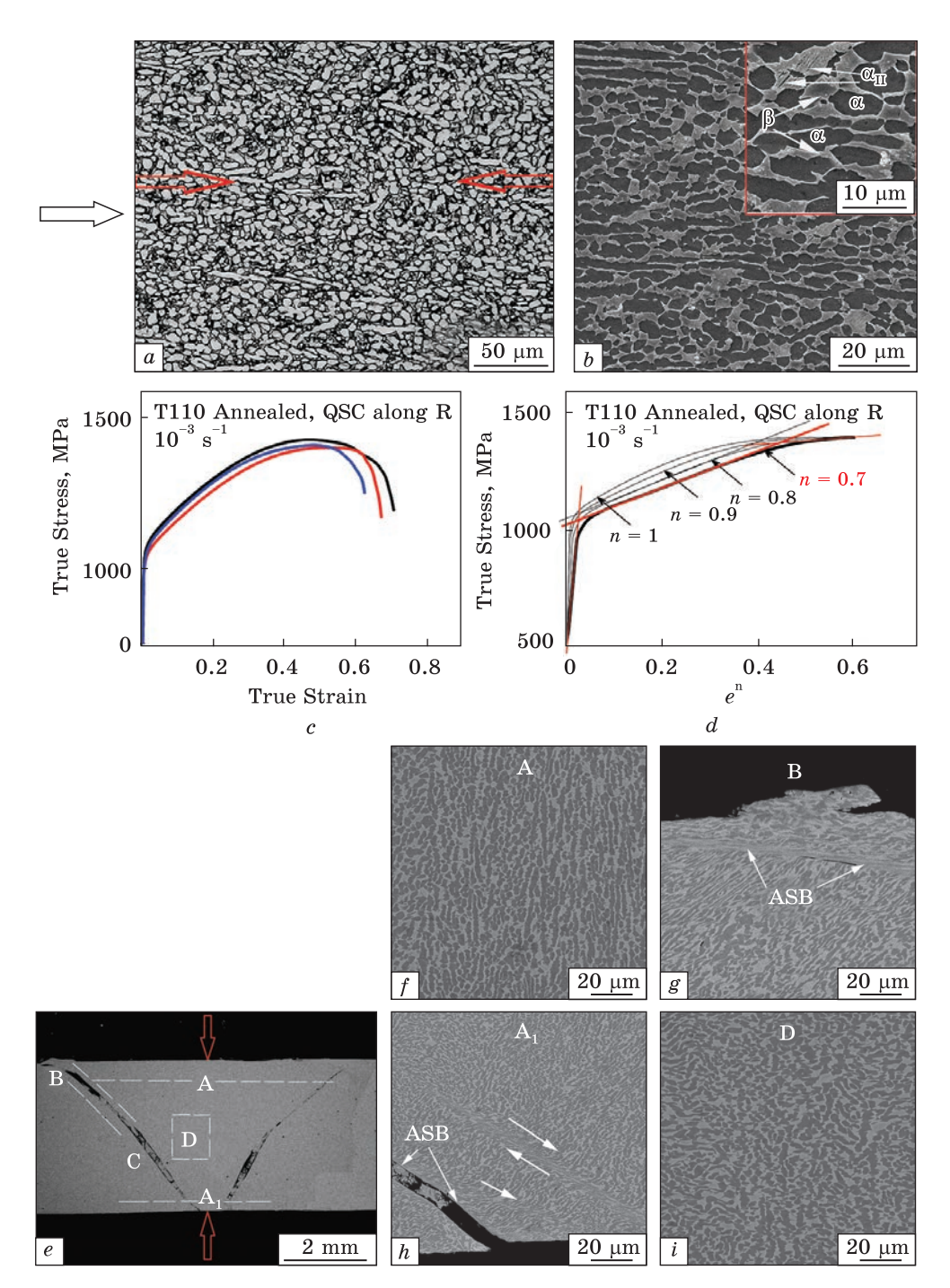
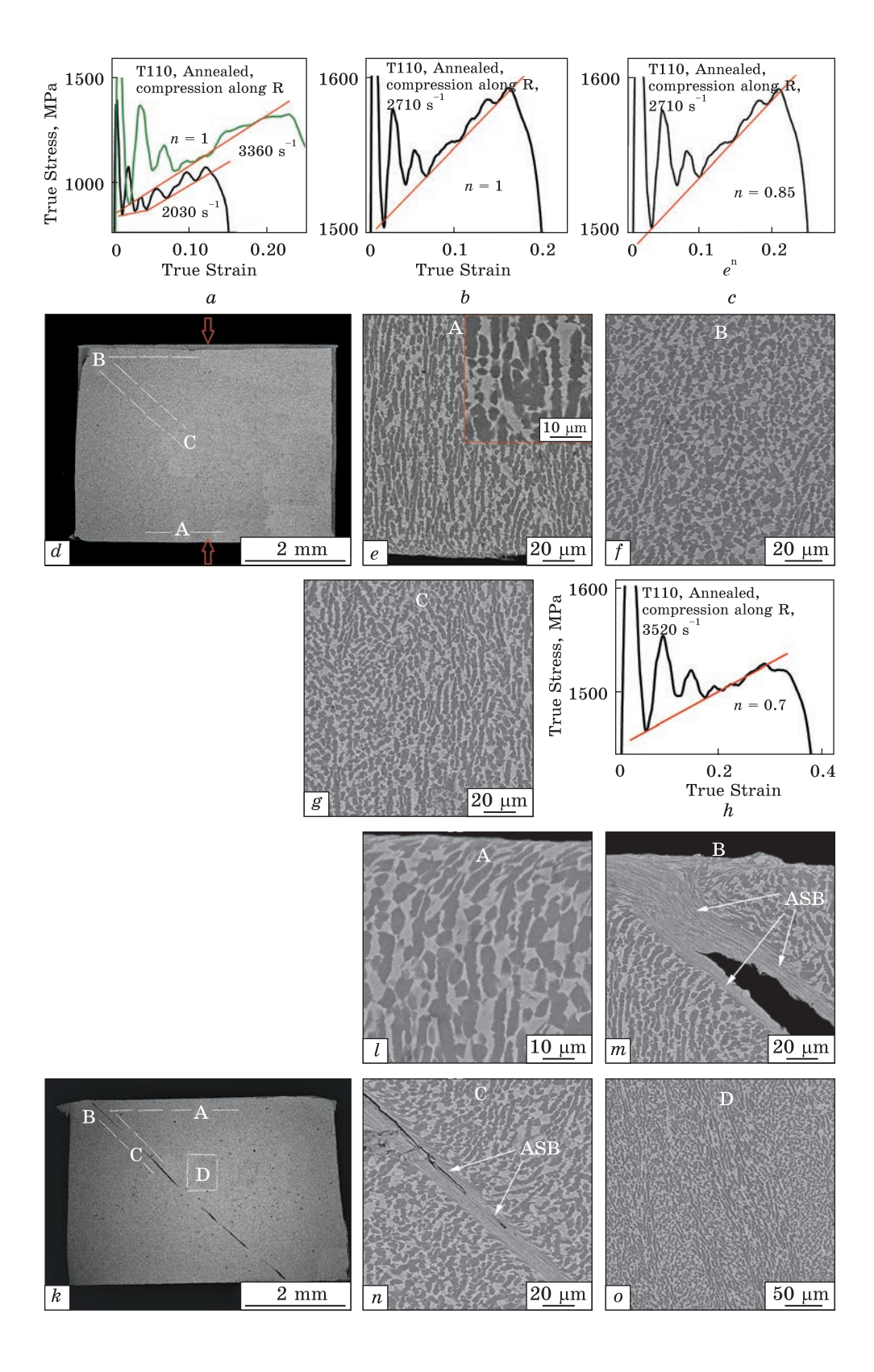


Fig. 18. Characterization of the T110 alloy in the annealed after rolling (initial) state: microstructure of OM (a), SEM-SE (b), strain hardening curves under quasi-static compression (c), reconstructed curves (d), general view (SEM, SE) of the sample after compression tests (e), features of the microstructure after quasi-static compression in the zones defined in e, h, f-i. The direction of compression is shown by arrows in a, e [32]

The homogeneous parts of the strain strengthening curves during dynamic compression of T110 alloy samples in the direction of rolling at the strain rate range of $2030-3360 \text{ s}^{-1}$ have been shown in Fig. 19, a, b. At first glance, most of the minima on these curves lie on straight lines that correspond to the value of the strain-strengthening exponent in Eq. (2) n = 1. Moreover, the first minima of samples compressed at higher strain rates of 2710 and 3520 s⁻¹ also almost fit on these straight lines. But a more thorough analysis shows that the majority of the minima, including the first one, at a speed of 2710 s⁻¹ are placed on straight lines that correspond to the value of n = 0.85 (Fig. 19, c). That is, it may mean that during dynamic compression, the mechanism of strain hardening (compared to quasi-static compression) is shifted towards the prevailing α -phase control. To clarify the obtained results, let us compare the initial microstructures in Fig. 18, a, b, with the microstructure after dynamic compression. The comparison shows that almost uniform elongated sections of the α -phase in the initial state turn into a chain queue with links that are separated from each other in some places (Fig. 19, e, inset). Such a transformation can occur when strengthening at high strain rates is mainly controlled by the α-phase (including the secondary one) with some contribution of the β-phase. The observed structure is formed by a complex interaction between slip in the α -phase and interphase slip. Because of the given data, it can be stated that the main contribution to the strengthening is given by sample sections A and C (Fig. 19, e, g).

Increasing the strain rate level to 3520 s⁻¹ leads to a decrease in the strain strengthening exponent to the value n = 0.7 (Fig. 19, h). For such a value of the exponent n, the largest number of minima of the deformation curve is superimposed on the straight line. The value of n indicates that the role of the β-phase in the strain strengthening mechanism increases as the strain rate increases. The microstructure (Fig. 19, l, m, o) definitely demonstrates that the layers of the β-phase located between the sections of the α -phase have practically no breaks in the direction of compression. At the same time, such breaks can be observed in the microstructure of the T110 alloy compressed with a strain rate of 2710 s⁻¹ (Fig. 19, e-g). The value of n = 0.7 indicates the deformation mechanism associated with the sliding of dislocations along the interphase boundaries. Then, it can be concluded that in the case of a strain rate of 3520 s⁻¹, the sliding of dislocations is more limited by the β -phase than in the case of compression with a strain rate of 2710 s⁻¹. In other words, increasing the velocity of dynamic compression of the annealed T110 alloy in the rolling direction causes a gradual increase in the role of the phase controlling the deformation mechanism, from α - to β -phase within one type of such a mechanism.

Compression of the annealed alloy in a direction perpendicular to the rolling direction is marked by a completely different mechanism of strain strengthening. Quasi-static compression is characterized by a strengthening



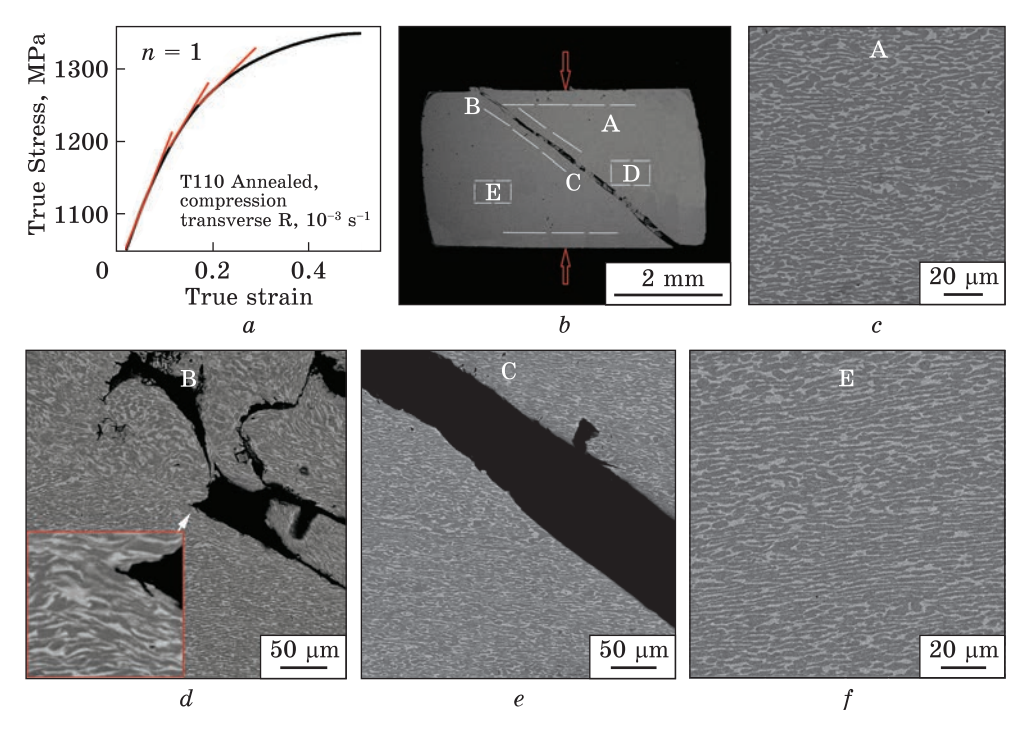


Fig. 20. Curve of quasi-static compression and microstructure of annealed T110 alloy in the direction perpendicular to the rolling direction: general view of the curve at the stage of homogeneous deformation (a); SEM, SE after compression (b-f). The direction of compression is vertical relative to the micrographs [32]

exponent n=1 (Fig. 20, a), which indicates the leading role of the α -phase in strengthening. This is not surprising since sections of the α -phase are strongly elongated perpendicular to the direction of compression (Fig. 18, b), and all other things being equal, the α -phase has a greater strengthening effect compared to the β -phase. The first part of the hardening curve is divided into three straight sections, which, according to the classics, successively correspond to the accumulation of chaotic dislocations at interphase boundaries (first), the transformation of these accumulations into heterogeneously distributed clusters (second) and, finally, the transformation of such clusters into non-misoriented dislocation cells (third). The last part of the curve is not described by any strengthening exponent. One possible explanation for this fact may be a transition from the effect of

[◄] Fig. 19. Dynamic compression curves and corresponding microstructures of the T110 alloy after compression in the annealed state in the rolling direction: the general appearance of the curves (a); compression curves at a strain rate of 2710 s⁻¹ at different values of the indicator n (b, c); SEM, SE after compression at this strain rate (d-g); compression curve at a strain rate of 3520 s⁻¹ (h); SEM, SE after compression at this rate (k-o). The rolling and compression directions are vertical to the micrographs [32]

dislocation inhibition by obstacles such as interphase boundaries to a strong interaction between inhibited dislocations, in which partial annihilation of dislocations occurs with the formation of misoriented cell boundaries and then grains. There is no confirmation of this at the moment.

Dynamic compression of the T110 alloy in the same annealed state in the direction perpendicular to the rolling direction is characterized by clear strengthening during compression (Fig. 21, a, g). Moreover, at a strain rate of 2570 s⁻¹, the strengthening exponent n = 0.8 indicates that compression deformation is controlled by both α - and β -phases simultaneously. This looks rather strange since such a value of n is typical if the deformation is controlled by sliding along the interphase boundaries when the phases are elongated along the compression direction. As has already been established, this is observed for the case when the directions of rolling, along which sections of the α-phase are elongated, and dynamic compression coincide. In this case, sections of the α -phase are elongated in the direction perpendicular to the direction of compression. A detailed study of the microstructure shows that after compression (Fig. 21, d-f) it has the following features: many continuous sections of the β-phase are elongated at 45° to the compression direction. This is especially noticeable in Fig. 21, a, c, that is, in areas adjacent to the edge of the sample to which the load was applied. In other words, in this case, deformation occurs by sliding in the β-phase, although the main strengthening is provided by the α -phase. Sliding in the β -phase occurs more easily than in the α -phase.

A slight increase in the strain rate to 2970 s⁻¹ leads to a hardening exponent of n = 1 (Fig. 21, f) and a significant change in the deformation mechanism, which becomes controlled by the α -phase. In addition, the shape of the curve also changed: the number of maxima decreased from 6 to 3, and the hardening coefficient decreased (the slope of the straight line describing the minima of the curve decreased). Such a significant change in the behaviour of the alloy with a slight increase in the velocity of dynamic compression is associated with the peculiarities of the change in the microstructure. First, continuous sections of the β-phase disappear, elongated at small angles relative to the direction of compression, which were observed at a strain rate of 2570 s⁻¹. Secondly, the regions of the α -phase, which are the main obstacles to the sliding of dislocations in the β -phase and which are elongated across the direction of compression, are 2-3 times longer than in the case of a strain rate of 2570 s⁻¹. Thus, the probability of dislocations bypassing the α -phase decreases several times. Therefore, the strengthening exponent for the dynamic compression corresponds to a deformation mechanism controlled by the α -phase.

The mechanical properties of the T110 alloy under compression after STA hardening are a matter of particular interest. The microstructure of this metallurgical state is presented in Fig. 22. There is a general elongation of the structural elements in the rolling direction (Fig. 22, a) and

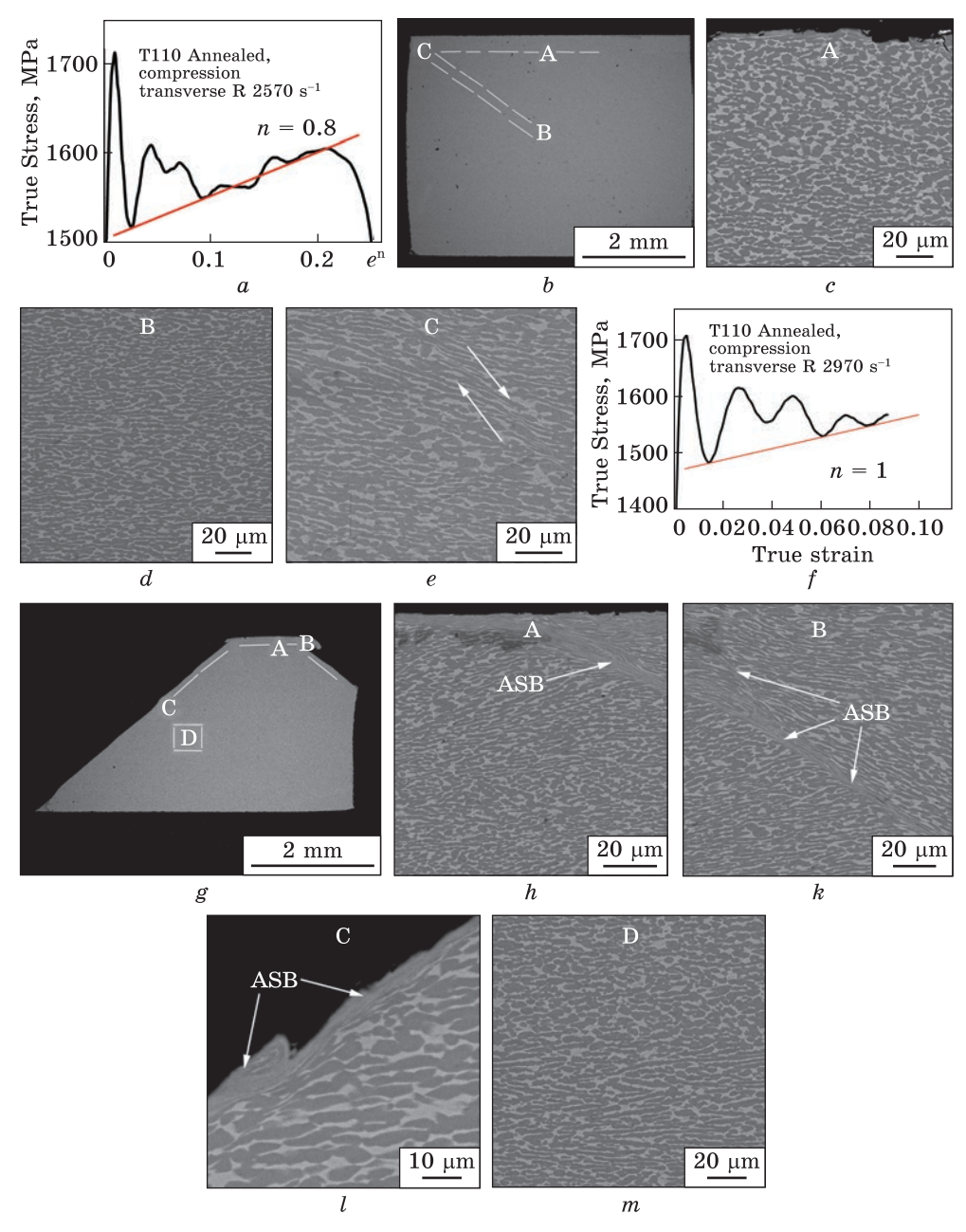


Fig. 21. Dynamic compression curves and microstructure of annealed T110 alloy in the direction perpendicular to the rolling direction: general view of the curve at the stage of uniform deformation at a strain rate of $2570 \, \text{s}^{-1}$ (a) and microstructure SEM, SE after compression (b-e); general view of the curve at the stage of uniform deformation at a strain rate of $2970 \, \text{s}^{-1}$ (f) and microstructure SEM, SE after compression (g-m). The direction of compression is vertical relative to the figure [32]

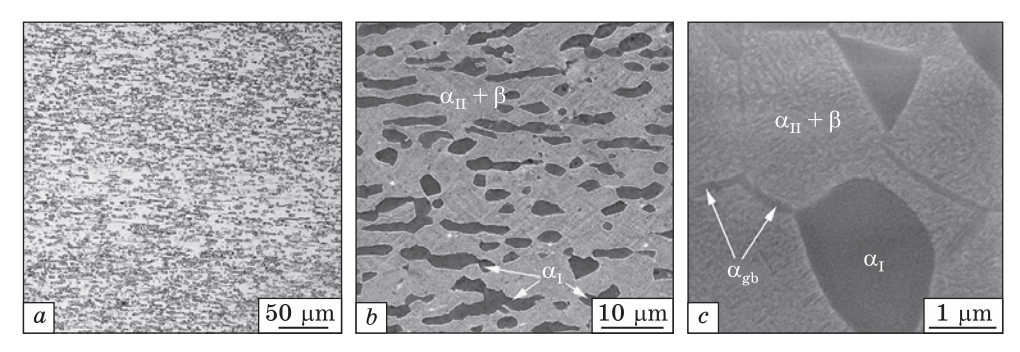


Fig. 22. Microstructure T110 annealed 850 °C after rolling in horizontal direction and STA-hardening: light microscopy (a), SEM BSE (b, c) [32]

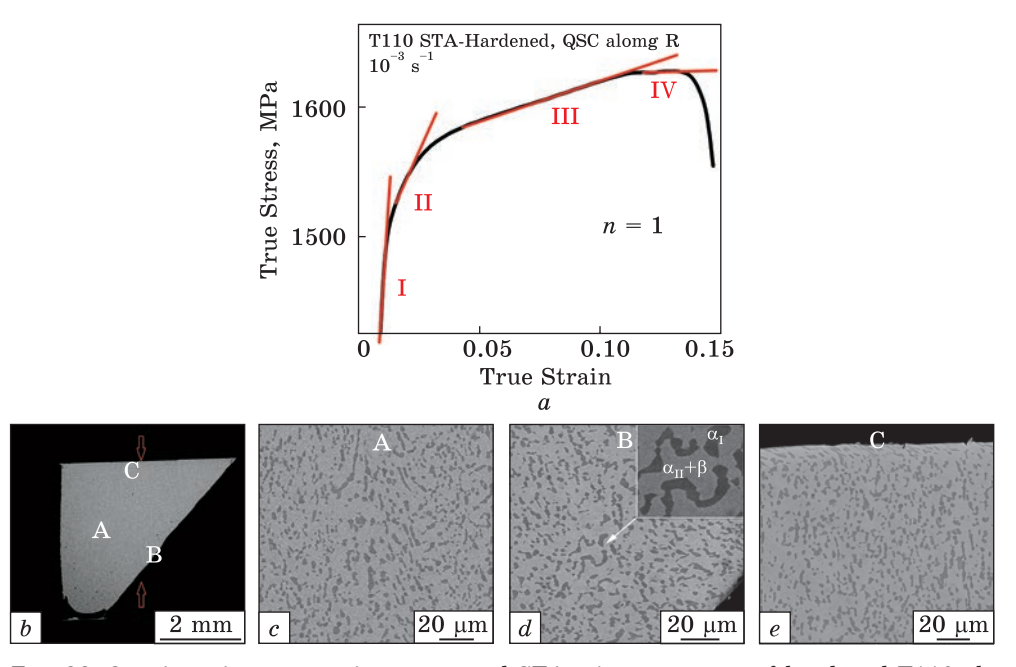


Fig. 23. Quasi-static compression curve and STA microstructure of hardened T110 alloy in the rolling direction: general view of the curve at the stage of homogeneous deformation with its decomposition according to Eq. (1) (a) microstructure SEM, SE after compression (b-e). The direction of compression is vertical relative to the micrographs [32]

specifically, elongation of the α -phase sections (Fig. 22, b). However, the main feature of the structure after STA hardening is the formation within the β -phase of a finely dispersed, uniformly distributed secondary α_{II} -phase (Fig. 22, c).

Such a microstructure affects the nature of the quasi-static compression curves (Fig. 23, a), which differ from the same compression curves of the non-hardened T110 alloy (Figs. 18, c and 20, a). Firstly, and this is

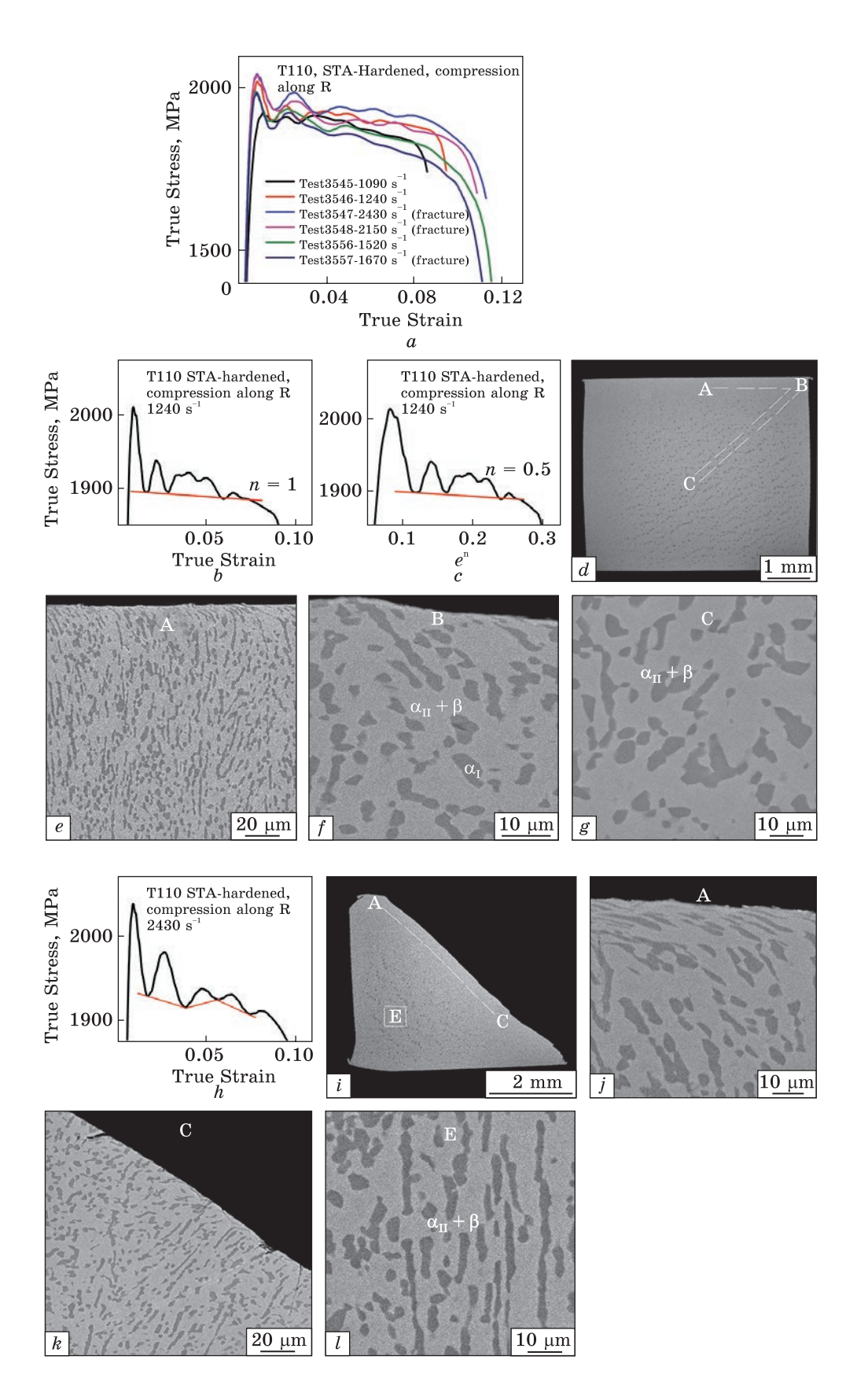
understandable, the hardened alloys have a significantly higher tensile strength (more than 1600 MPa against 1400 MPa). Secondly, the strengthening exponent n=1 indicates that the deformation mechanism is controlled by the α -phase. Judging by how curved the sections of the primary α -phase become after compression (Fig. 23, c, d), it is clear that they, along with the secondary α -phase, control the deformation and strengthening of quasi-static compression. Thirdly, the curve at n=1 is well divided into four straight sections. The first three sections correspond to the usual standard types of microstructures that are formed on them during deformation. However, the fourth section, where there is practically no strengthening, is not quite ordinary. This means that dislocations that form during compression annihilate with dislocations formed at previous stages of deformation.

In addition, since at the third stage a structure of non-misoriented dislocation cells is formed, we can assume that these cells at the fourth stage turn into misoriented low-angle ones, after which a sharp softening and destruction occurs.

Dynamic compression along the rolling direction of STA-hardened samples is characterized by the virtual absence of a conditionally homogeneous strengthening stage. This is apart from the sharp first maximum (Fig. 24, a), which demonstrates a significant increase in compression strength compared to the same compression of an unhardened alloy (about 2000 MPa *versus* 1700 MPa). In the rest of the curve, strain softening occurs up to the fracture.

An attempt was made to represent such compression curves with softening in the form of an exponential function, as was done for curves with conditionally homogeneous stages of strengthening. The results for a strain rate of $1240 \, \mathrm{s}^{-1}$ are presented in Fig. 24, b, c. It follows that the representations are absolutely the same for both the case n=1 and 0.5. That is, the symmetry of the curve relative to the approximating straight line is also the same for these extreme cases of approximation. This means that the formal transfer of the concept developed for compression curves with pronounced, conditionally homogeneous stages of strengthening does not work for hardened alloys when there is no pronounced stage of strengthening. Obviously, in the case of softening, a completely different approach must be developed for analysing stress-strain curves in general and for dynamic compression in particular.

However, based on consideration of the microstructure, assumptions can be made about an element of the structure controlling deformation and softening. The structure after compression at a strain rate of 1240 s^{-1} represents particles of the α -phase elongated along the rolling direction, rather sparsely distributed in a volume consisting of the β -phase with dispersed sub-nanoparticles of the secondary α -phase (Fig. 24, e, f, g). From this, it follows that the mechanism of deformation (and softening) by dy-



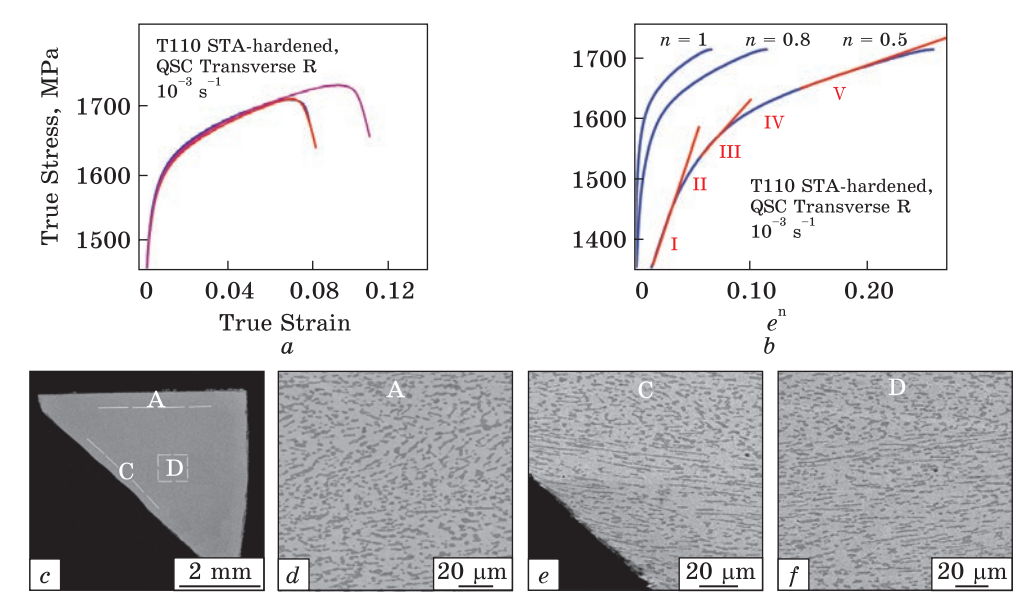


Fig. 25. Quasi-static compression curves and microstructure of STA hardened T110 alloy in the direction perpendicular to the rolling direction; general view of the curves (a); representation of the curve according to Eq. (1) for different values of n (b); microstructure, SEM SE after compression (c-f). The direction of compression is vertical relative to the micrographs [32]

namic compression in this case is controlled either by the secondary α -phase, or by sliding along interphase boundaries, or by their combined action. Most likely, nanoparticles of the secondary α -phase near the interphase boundaries dissolve under the influence of high stresses and dislocation glide velocities. This creates a condition that promotes the softening of the alloy by sliding along the interphase boundaries. However, this is only an assumption, for which there is no evidence yet.

Increasing the strain rate by almost a factor of 2 (strain rate 2430 s⁻¹) leads to a small intermediate short-term strengthening (Fig. 24, h), in contrast to stable softening at a strain rate of 1240 s⁻¹. The most likely reason for this behaviour of the alloy is the appearance of adiabatic shear bands (ASB), which localize the deformation. The formation of ASBs is precisely preceded by a short stage of slight strengthening, after which intense softening occurs.

Fig. 24. Dynamic compression curves and microstructure of STA hardened T110 alloy in the rolling direction: general view of curves for different strain rate levels (a); representation of the compression curve at 1240 s⁻¹ according to Eq. (1) with n = 1 (b) and n = 0.5 (c); microstructure SEM, SE after compression at 1240 s⁻¹ (d−g); general view of the compression curve at a strain rate of 2430 s⁻¹ (h); microstructure, SEM SE after compression at 2430 s⁻¹ (i−l). The direction of compression is vertical relative to the micrographs (shown by arrows) [32]

The STA-hardened T110 alloy exhibits very interesting deformation properties under quasi-static compression in the direction perpendicular to the rolling direction (Fig. 25). The deformation curves shown in Fig. 25, a demonstrate stable strengthening at the homogeneous stage. This stage, reconstructed according to Eq. (1), is best described by the exponent n = 0.5. It is interesting to note that after the first rectilinear section, but, before the third, there is a section, which is not described by a straight line and remains nonlinear. The same curve history is observed after the third section, which is also rectilinear: the fourth section is curved. The fifth section is strictly rectilinear. It is appropriate to assume here that the rectilinear sections correspond to clearly visible formations of the dislocation structure: the first section corresponds to the chaotic distribution of dislocations, the third to the formation of dislocation tangles and condensations, and in the fifth section, non-disoriented dislocation cells are formed. The reason for the nonlinear transitions from a chaotic distribution of dislocations to tangles and condensations, as well as from tangles to cells, most likely lies in the formation of thin β-phase interlayers free of the secondary α-phase during deformation, which determines the deformation mechanism. Most likely, this occurs due to the dissolution of secondary α-phase nanoparticles under the action of high mechanical stresses created by dislocations that cannot overcome transverse interphase boundaries. It can be assumed that most of these β -phase interlayers, free of secondary α -phase particles, appear in regions A and B of the sample (Fig. 24, b). However, based on the available structural data, confirmation of this cannot be found at present.

Dynamic compression of STA-hardened samples deformed transverse to the rolling direction, as well as similar compression along the rolling direction, is characterized by a general tendency toward softening after a sharp initial stage of hardening (Fig. 26, a). However, there is a significant difference. The curves with transverse compression versus rolling, regardless of the strain rate, after a sharp initial maximum, are divided into two large regions. The first demonstrates general softening, while the second contains elements of strengthening. This is especially noticeable with a separate increase in the curves, for example, with strain rates of 1170 and 1220 s⁻¹ (Fig. 26, b, g). In the case of dynamic compression of samples with longitudinal compression relative to the rolling direction, softening is observed throughout the entire deformation after a sharp maximum (Fig. 24, a-c).

It can be assumed that the main reason for both softening in the first region and strengthening in the second is the appearance of small nanoscopic areas of pure β -phase in the vicinity of the interphase boundaries. This most likely occurs due to the dissolution of the secondary α -phase under the action of high dynamic stresses at the interphase boundaries. However, if relative to the first region of the deformation curve, it can be

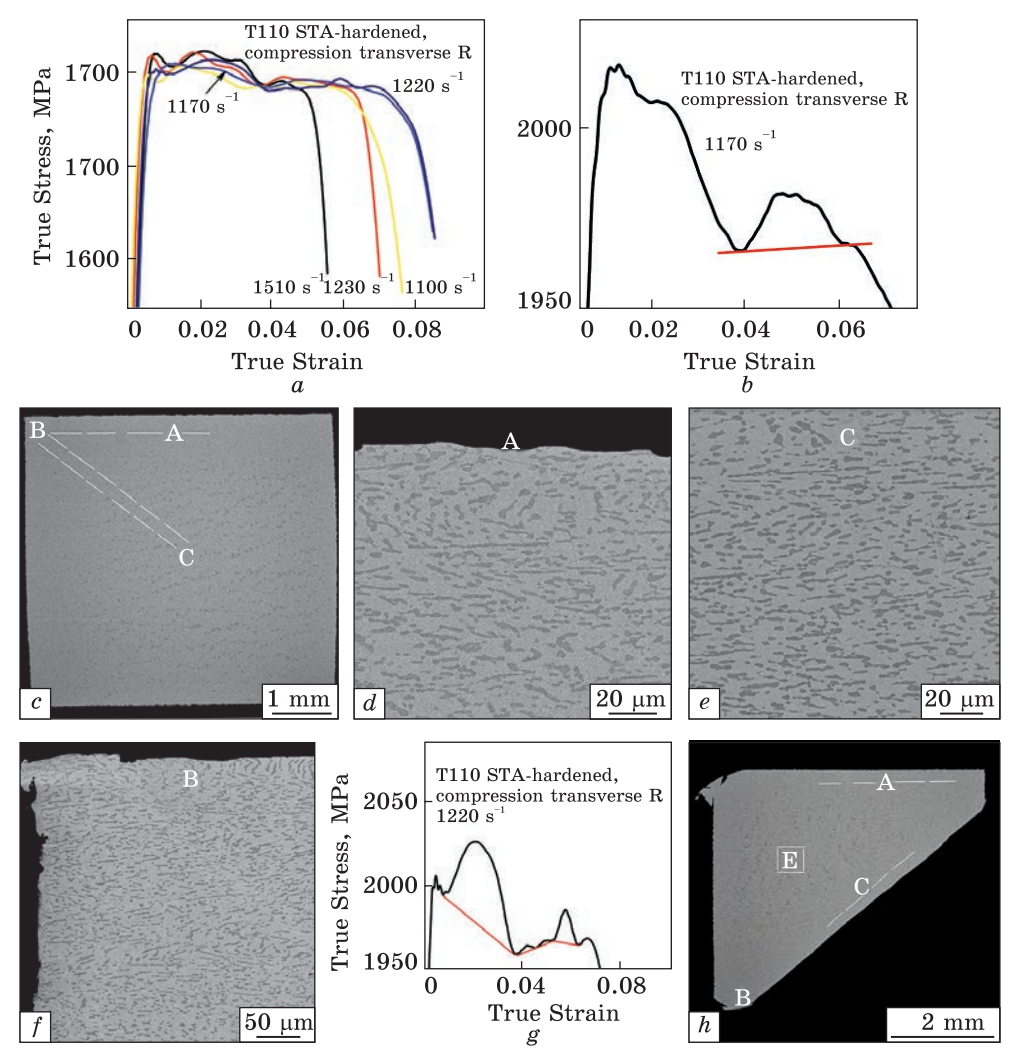
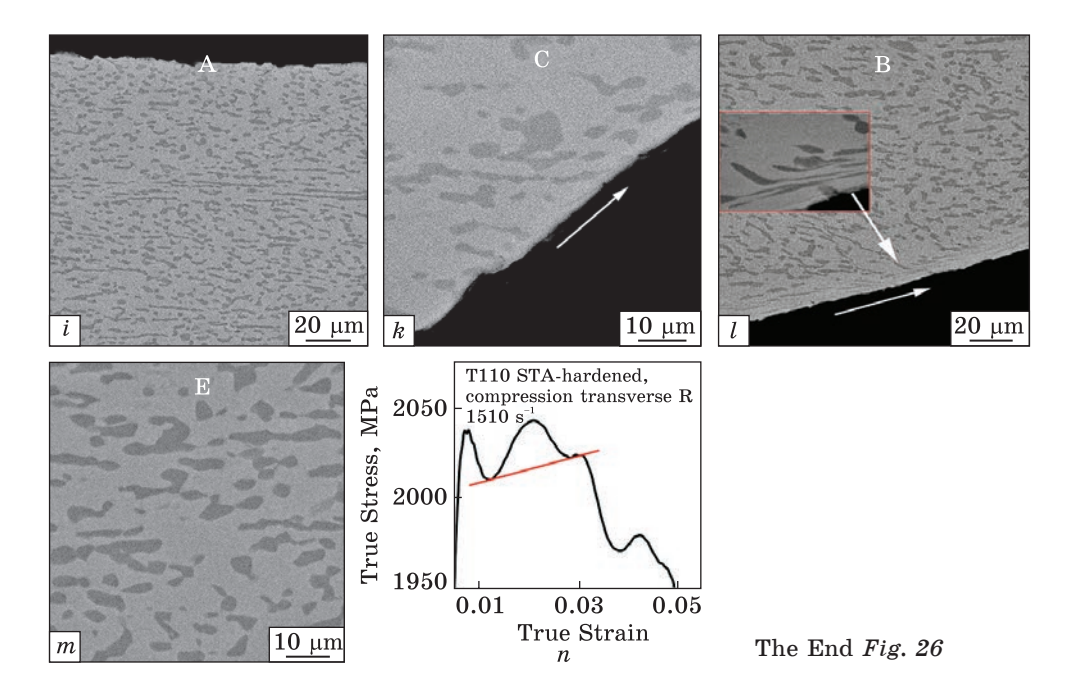


Fig. 26. Dynamic compression curves and microstructure of STA hardened T110 alloy in the direction perpendicular to the rolling direction: general view of the compression curves of samples at different strain rates (a); general view of the compression curve at a strain rate of 1170 s^{-1} (b) and the microstructure of the SEM, SE after compression at this strain rate level (c-f); general view of the compression curve at a strain rate of 1220 s^{-1} (f) and the microstructure of the SEM, SE after compression at this strain rate level (g-m); general view of the compression curve at a strain rate of 1510 s^{-1} . The direction of compression is vertical relative to the micrographs [32]

assumed that such sections of the β -phase have the form of nanospherical formations, then during the deformation process in the second region, such nanospheres merge into extended sections located along the α - β -interphase boundaries. Spheres are not effective obstacles since disloca-



tions can freely bypass them. However, the linear nano-β-phase adjacent to the interface can be such an obstacle. That is why softening is observed in the second region. Moreover, with an increase in strain rate to 1220 s⁻¹, the second region appears in the form of several minima, which lie on a straight line with the strengthening exponent n=1 (Fig. 26, g). In other words, in the second region, β-phase nanolayers are formed, which cause strengthening, but do not determine the mechanism of strain strengthening. The latter is determined by the primary α -phase. It is not yet possible to explain this effect due to the lack of an available model of the observed behaviour and the necessary experimental structural data. It is interesting to note that with an increase in the strain rate to 1510 s⁻¹, the region of primary softening is completely absent (Fig. 26, n). There is an area of primary strengthening and final softening. Conclusion: with an increase in the strain rate of dynamic compression of STA-hardened samples of the T110 allow tested transverse to the rolling direction, there is a tendency towards partial strain strengthening while maintaining the general nature of softening.

3. Conclusions

The features of deformation and strengthening during quasi-static and high-strain rate compression of some titanium alloys with different initial structural states and composites on the base of Ti64 alloy strengthened with TiC and TiB particles were studied. Strain hardening curves have

been processed according to the principle developed by V.F. Moiseev for tension metals and alloys. According to this approach, exponents and coefficients of strain hardening were determined. By comparing these features with structural changes according to optical microscopy (OM) and scanning electron microscopy (SEM), it was determined what structural elements (phases, defect structure) and how they control and influence the mechanism of deformation and hardening at a homogeneous stage of compression deformation. It was found for the first time that the approach developed for the analysis of tensile deformation curves can be successfully applied to the analysis of curves not only of quasi-static compression deformation but also for high-strain rate compression.

The peculiarity of the approach to the analysis of the curves of highstrain rate compression of titanium alloys, which have an oscillating character at the stage of homogeneous hardening, is that the curves are analysed according to their minima since these minima correspond to the relaxation of elastic stresses in the process of dynamic deformation.

In most cases, the mechanisms of deformation and strengthening of titanium alloys under quasi-static and high-strain rate compression (as well as the types of curves) differ.

It was found that, depending on the metallurgical state and structural features, in the two-phase $\alpha+\beta$ -titanium alloy based on Ti64 composition the deformation and strengthening mechanism can be controlled either by one of the phases, when slip and strengthening occur in one phase, or by two phases simultaneously and equally, or when deformation and strengthening occur along the interphase boundary. In turn, in pure titanium, the role of the second phase can be played by twins that arise during compression. In addition, twins also appear in the two-phase alloy. Twins provide a rotational deformation mode, while in the α - and β -phases, a shear deformation mode takes place.

The introduction of micronsize TiB or TiC strengthening particles by powder metallurgy into the Ti64 composition-based alloy forms a metalmatrix (MMC) three-phase composite with a lamellar structure and residual pores. The deformation mechanisms of such composites under quasistatic and dynamic compression are characterized by specific features. The strengthening mechanism of the MMC at the homogeneous stage under quasi-static compression is determined by the beta phase surrounding the boride or carbide particles. Such an alloy under dynamic compression can either strengthen or soften depending on the content of TiB or TiC particles and the compression rate.

Two-phase more alloyed titanium alloy T110, subjected to a series of successive treatments, including rolling in the region below beta-transformation temperature (T_{β}), has microstructural features that determine the mechanisms of deformation, strengthening, and softening during quasistatic and dynamic compression. Such features are large angles of misori-

entation of interphase boundaries and a secondary α -phase. Depending on the orientation of the compression direction relative to the rolling direction and the compression rate, the mechanisms of deformation and hardening determined from the compression curves can change dramatically. In alloys subjected to additional STA-hardening, pronounced softening occurs during dynamic compression, but with an increase in the strain rate, areas of strain hardening appear.

Acknowledgements. The entire complex of presented and analysed in this paper studies of the mechanical behaviour of titanium-based materials was carried out under the Agreement on Scientific and Technical Cooperation between G.V. Kurdyumov Institute for Metal Physics of the N.A.S. of Ukraine (Kyiv, Ukraine) and Jarosław Dąbrowski Military University of Technology (Warsaw, Poland) during 2019–2024. The authors express their gratitude to their colleagues, who took part in various ways possible at certain stages of the research, namely: Dr. Eng. J. Senkiewicz, MSc. Eng. K. Cieplak, and MSc. Eng. P. Dziewit (Jarosław Dąbrowski Military University of Technology); Prof. S. Prikhodko (University of California, Los Angeles, U.S.A.); Drs. D. Savvakin, O. Stasyuk, V. Bondarchuk, D. Oryshych, M. Skoryk, and Mr. B. Melamed (G.V. Kurdyumov Institute for Metal Physics of the N.A.S. of Ukraine).

REFERENCES

- 1. N.F. Mott, The mechanical properties of metals, *Proc. Phys. Soc. B*, **64**, No. 9: 729-742 (1951);
 - https://doi.org/10.1088/0370-1301/64/9/301
- 2. A.S. Argon, Mechanical properties of single-phase crystalline media: deformation at low temperatures, *Physical Metallurgy* (Eds. R.W. Cahn and P. Haasen) (Elsevier: 1996), Ch. 21, p. 1877–1955;
 - https://doi.org/10.1016/b978-044489875-3/50026-0
- 3. P. Haasen, Mechanical properties of solid solutions, *Physical Metallurgy* (Eds. R.W. Cahn and P. Haasen) (Elsevier: 1996), Ch. 23, p. 2009–2073; https://doi.org/10.1016/b978-044489875-3/50028-4
- J.-L. Strudel, Mechanical properties of multiphase alloys, *Physical Metallurgy* (Eds. R.W. Cahn and P. Haasen) (Elsevier: 1996), Ch. 25, p. 2105–2206; https://doi.org/10.1016/b978-044489875-3/50030-2
- R.E. Smallman and A.H.W. Ngan, Plastic deformation and dislocation behaviour, Modern Physical Metallurgy, Ch. 9, p. 357-414 (2014); https://doi.org/10.1016/b978-0-08-098204-5.00009-2
- X.Li, L. Lu, J. Li, X. Zhang, and H. Gao, Mechanical properties and deformation mechanisms of gradient nanostructured metals and alloys, *Nat. Rev. Mater.*, 5, 706–723 (2020);
 - https://doi.org/10.1038/s41578-020-0212-2
- 7. V.I. Trefilov, V.F. Moiseev, and E.P. Pechkovsky, Deformation hardening and fracture of polycrystalline materials (Kiev: Naukova Dumka: 1989) (in Russian).
- 8. V.F. Moiseev, Effective exponent of deformation strengthening the metals, *Metallofiz. Noveishie Tekhnol.*, 23, 387–399 (2001) (in Russian).

- 9. Yu.N. Podrezov and S.A. Firstov, Two approaches to the analysis of strain hardening curves, *High Pressure Physics and Engineering*, **16**: 37–48 (2006) (in Russian);
 - https://dspace.nbuv.gov.ua/handle/123456789/70256
- U.F. Kocks and H. Mecking, Physics and phenomenology of strain hardening: the FCC case, *Prog. Mater. Sci.*, 48, No. 3: 171-273 (2003); https://doi.org/10.1016/S0079-6425(02)00003-8
- 11. U. Zwikker, *Titan und Titanlegirungen* (Berlin-Heidelberg: Springer: 1974); https://doi.org/10.1007/978-3-642-80587-5
- 12. G. Lutjering and J.C. Williams, *Titanium* (Berlin-Heidelberg: Springer: 2007); https://doi.org/10.1007/978-3-540-73036-1
- 13. A.V. Kotko, V.F. Moiseev, E.P. Pechkovskij, I.V. Moiseeva, and V.K. Pishchak, Special features of the plastic deformation of multiphase titanium alloys, *Metallofiz. Noveishie Tekhnol.*, 23: 1013–1027 (2001) (in Russian).
- 14. V.F. Moiseev, I.V. Moiseeva, and V.K. Pishchak, Influence of α and β-phases on low- and high-temperature strength of titanium alloy VT 6, *Metallofiz. Noveishie Tekhnol.*, 25: 193–203 (2003) (in Russian).
- A.I. Dekhtyar, M.V. Matviychuk, I.V. Moiseeva, and D.G. Savvakin, Strain hardening and fracture of VT-6 alloy synthesized by the method of powder metallurgy, *Mater. Sci.*, 44: 429–434 (2008); https://doi.org/10.1007/s11003-008-9097-8
- 16. A.V. Kotko, Deformation hardening of titanium alloys, *Modern Problems of Physical Materials Science: Collective Scientific Works* (Kyiv: Institute for Problems of Materials Science of the N.A.S. of Ukraine: 2013), vol. 22, p. 94–102 (in Russian).
- 17. A.I. Dekhtyar, I.V. Moiseeva, and D.G. Savvakin, Deformation and fracture of alloys synthesized by powder metallurgy, *Metallofiz. Noveishie Tekhnol.*, **35**: 889–908 (2013) (in Russian).
- 18. A.I. Dekhtyar, V.I. Bondarchuk, V.V. Nevdacha, and A.V. Kotko, The effect of microstructure on porosity healing mechanism of powder near- β titanium alloys under hot isostatic pressing in $\alpha+\beta$ -region: Ti-10V-2Fe-3Al, *Mater. Charact.*, **165**: 110393 (2020);
 - https://doi.org/10.1016/j.matchar.2020.110393
- C.M. Sellars and W.J. McTegart, On the mechanism of hot deformation, *Acta Metall.*,
 No. 9: 1136–1139 (1966);
 https://doi.org/10.1016/0001-6160(66)90207-0
- H.J. McQueen and W.J. McGregor, The deformation of metals at high temperatures, Scientific American, 232, No. 4: 116-125 (1975); https://www.jstor.org/stable/24949778
- S.L. Semiatin, V. Seetharaman, and I. Weiss, The thermomechanical processing of alpha/beta titanium alloys, JOM, 49: 33-39 (1997); https://doi.org/10.1007/BF02914711
- 22. I. Weiss and S.L. Semiatin, Thermomechanical processing of beta titanium alloys an overview, *Mater. Sci. Eng. A*, 243, Nos. 1–2: 46–65 (1998); https://doi.org/10.1016/S0921-5093(97)00783-1
- 23. V. Tuninettia, G. Gillesa, V. Pйron-Lьhrsa, and A.M. Habrakena, Compression test for metal characterization using digital image correlation and inverse modeling, *Procedia IUTAM*, 4: 206–214 (2012);
 - https://doi.org/10.1016/j.piutam.2012.05.022
- 24. Y.D. Wang, A. Vadon, and J.J. Heizmann, Room temperature compression textures and deformation mechanisms of Ti-46Al-2V alloy, *Mater. Sci. Eng. A*, 222, No.

- 1:70-75(1997);
- https://doi.org/10.1016/S0921-5093(96)10380-4
- P.R. Sreenivasan and S.K. Ray, Mechanical testing at high strain rates, Encyclopedia of Materials: Science and Technology (New York, USA: Elsevier: 2001, p. 5269–5271; https://doi.org/10.1016/B0-08-043152-6/00919-0
- J.S. Pigott, N. Velisavljevic, E.K Moss, D. Popov, C. Park, J.A. Van Orman, N. Draganic, Y.K. Vohra, and B.T. Sturtevant, J. Phys.: Condens. Matter, 32, No. 12: 12LT02 (2020);
 - https://doi.org/10.1088/1361-648X/ab5e6e
- 27. B. Morrow, R. Lebensohn, C. Trujillo, D.T. Martinez, F. Addessio, C.A. Bronkhorst, T. Lookman, and E. Cerreta, E. Characterization and modeling of mechanical behavior of single crystal titanium deformed by split-Hopkinson pressure bar. *Int. J. Plast.*, 82: 225–240 (2016);
 - https://doi.org/10.1016/j.ijplas.2016.03.006
- W. Yin, F. Xu, O. Ertorer, Z. Pan, X. Zhang, L. Kecskes, E.J. Lavernia, and Q. Wei, Mechanical behavior of microstructure engineered multi-length-scale titanium over a wide range of strain rates, *Acta Mater.*, 61, No. 10: 3781-3798 (2013); https://doi.org/10.1016/j.actamat.2013.03.011
- 29. T. Zhou, J. Wu, J. Che, Y. Wang, and X. Wang, Dynamic shear characteristics of titanium alloy Ti-6Al-4V at large strain rates by the split Hopkinson pressure bar test. *Int. J. Impact Eng.*, **109**: 167-177 (2017); https://doi.org/10.1016/j.ijimpeng.2017.06.007
- 30. Y. Guo, Q. Ruan, S. Zhu, Q. Wei, J. Lu, B. Hu, X. Wu, and Y. Li, Dynamic failure of titanium: Temperature rise and adiabatic shear band formation. *J. Mech. Phys. Solids*, 135: 103811 (2020); https://doi.org/10.1016/j.jmps.2019.103811
- P.E. Markovsky, J. Janiszewski, V.I. Bondarchuk, O.O. Stasyuk, D.G. Savvakin, M.A. Skoryk, K. Cieplak, P. Dziewit, and S.V. Prikhodko, Effect of strain rate on microstructure evolution and mechanical behavior of titanium-based materials, Metals, 10,No. 11: 1404 (2020); https://doi.org/10.3390/met10111404
- 32. P.E. Markovsky, J. Janiszewski, V.I. Bondarchuk, O.O. Stasyuk, K. Cieplak, and O.P. Karasevska, Effect of strain rate on mechanical behavior and microstructure evolution of Ti-based T110 alloy, *Metallog., Microstruct., Anal.*, 10: 839–861 (2021);
 - https://doi.org/10.1007/s13632-021-00797-9
- 33. P.E. Markovsky, J. Janiszewski, S.V. Akhonin, V.I. Bondarchuk, V.J. Berezos, K. Cieplak, O.P., Karasevska, M.A. Skoryk, Mechanical behavior of Ti-15Mo alloy produced with electron-beam cold hearth melting depending on deformation rate and in comparison with other titanium alloys, *Prog. Phys. Met.*, 23, No. 3: 438–475 (2022):
 - https://doi.org/10.15407/ufm.23.03.438
- 34. P.E. Markovsky, J. Janiszewski, O.O. Stasyuk, V.I. Bondarchuk, D.G. Savvakin, M.A. Skoryk, K. Cieplak, D. Goran, P. Soni, and S.V. Prikhodko, Mechanical behavior of titanium based metal matrix composites reinforced with TiC or TiB particles under quasi-static and high strain-rate compression, *Materials*, 14, No. 22: 6837 (2021);
 - https://doi.org/10.3390/ma14226837
- 35. P.E. Markovsky, J. Janiszewski, D.G. Savvakin, O.O. Stasiuk, V.I. Bondarchuk, K. Cieplak, P. Baranowski, and S.V. Prikhodko, Mechanical behavior of bilayer structures of Ti64 alloy and its composites with TiC or TiB under quasi-static and

- dynamic compression, *Materials and Design*, **223**: 111205 (2022); https://doi.org/10.1016/j.matdes.2022.111205
- 36. P.E. Markovsky, J. Janiszewski, O.I. Dekhtyar, M. Mecklenburg, and S.V. Prikhodko, Deformation mechanism and structural changes in the globular Ti-6Al-4V alloy under quasi-static and dynamic compression. to the question of the controlling phase in the deformation of $\alpha + \beta$ titanium alloys, *Crystals*, 12, No. 5: 645 (2022); https://doi.org/10.3390/cryst12050645
- 37. H. Kolsky, Propagation of stress waves in linear viscoelastic solids, *J. Acoust. Soc. Am.*, 37: 1206–1207 (1965); https://doi.org/10.1121/1.1939562
- 38. H. Kolsky, Stress waves in solids, J. Sound Vib., 1: 88–110 (1964); https://doi.org/10.1016/0022-460x(64)90008-2
- 39. W. Chen and B. Song, Split Hopkinson (Kolsky) Bar: Design, Testing and Applications (Berlin-Heidelberg: Springer: 2011); https://doi.org/10.1007/978-1-4419-7982-7
- 40. Y. Guo, Q. Ruan, S. Zhu, Q. Wei, J. Lu, B. Hu, X. Wu, and Y. Li, Dynamic failure of titanium: Temperature rise and adiabatic shear band formation, *J. Mech. Phys. Solids*, 135: 103811 (2020); https://doi.org/10.1016/j.jmps.2019.103811
- 41. M. Deguchi, M.S. Yamasaki, M. Mitsuhara, H. Nakashima, G. Tsukamoto, and T. Kunieda, Tensile deformation behaviors of pure Ti with different grain sizes under wide-range of strain rate, *Materials*, 16, No. 2: 529 (2023); https://doi.org/10.3390/ma16020529
- 42. G. Lütjering, Influence of processing on microstructure and mechanical properties of $(\alpha + \beta)$ titanium alloys, *Mater. Sci. Eng. A*, 243, Nos. 1–2: 32–45 (1998); https://doi.org/10.1016/S0921-5093(97)00778-8
- 43. T.R. Jones, Army Research Laboratory, Report ARL-CR-0533 (February 2004), p. 19.
- 44. P.E. Markovsky, Mechanical behavior of titanium alloys under different conditions of loading, *Mater. Sci. Forum*, **941**: 839–844 (2018); https://doi.org/10.4028/www.scientific.net/MSF.941.839
- 45. J. Li, L. Liu, Sh. Xu, J. Zhang, and W. She, First-principles study of mechanical, electronic properties and anisotropic deformation mechanisms of TiB under uniaxial compressions, *Appl. Phys. A*, **125**: 222 (2019); https://doi.org/10.1007/s00339-019-2523-y
- 46. O.M. Ivasishin, P.E. Markovsky, D.G. Savvakin, O.O. Stasyuk, S.D. Sitzman, M. Norouzi Rad, and S. Prikhodko, Multi-layered structures of Ti-6Al-4V alloy and TiC and TiB composites on its base fabricated using blended elemental powder metallurgy, J. Mater. Process. Technol., 269: 172–181 (2019); https://doi.org/10.1016/j.jmatprotec.2019.02.006
- 47. O.M. Ivasishin and V.S. Moxon, Low cost titanium hydride powder metallurgy, *Titanium Powder Metallurgy, Science, Technology and Applications*; (Eds. M. Qian, S.H. Froes) (Amsterdam, the Netherlands: Elsevier: 2015); Ch. 8, p. 117–148; https://doi.org/10.3390/met10050682
- 48. P.E. Markovsky, O.M. Ivasishin, D.G. Savvakin, V.I. Bondarchuk, and S. Prikhodko, Mechanical behavior of titanium-based layered structures fabricated using blended elemental powder metallurgy, *J. Mater. Eng. Perform.*, 28: No. 9: 5772–5792 (2019);
 - https://doi.org/10.1007/s11665-019-04263-0
- L. Gibson and M. Ashby, Cellular Solids: Structure and Properties (Cambridge: Cambridge University Press: 1997); https://doi.org/10.1017/CBO9781139878326

- 50. A. Suzuki, N. Kosugi, N. Takata, and M. Kobashi, Microstructure and compressive properties of porous hybrid materials consisting of ductile Al/Ti and brittle Al₃Ti phases fabricated by reaction sintering with space holder, *Mater. Sci. Eng. A*, 776: 139000 (2020);
 - https://doi.org/10.1016/j.msea.2020.139000
- 51. P.E. Markovsky, J. Janiszewski, O.O. Stasyuk, D.G. Savvakin, D.V. Oryshych, and P. Dziewit, Mechanical energy absorption ability of titanium-based porous structures produced by various powder metallurgy approaches, *Mater.*, **16**: 3530 (2023); https://doi.org/10.3390/ma16093530
- 52. P.E. Markovsky, D.V. Kovalchuk, S.V. Akhonin, S.L. Schwab, D.G. Savvakin, O.O. Stasiuk, D.V. Oryshych, D.V. Vedel, M.A. Skoryk, and V.P. Tkachuk, New Approach for Manufacturing Ti-6Al-4V+40% TiC Metal-Matrix Composites by 3D Printing Using Conic Electron Beam and Cored Wire. Pt. 1: Main Features of the Process, Microstructure Formation and Basic Characteristics of 3D Printed Material, Prog. Phys. Met., 24, No. 4: 715-740 (2023); https://doi.org/10.15407/ufm.24.04.715
- 53. P.E. Markovsky, D.V. Kovalchuk, J. Janiszewski, B. Fikus, D.G. Savvakin, O.O. Stasiuk, D.V. Oryshych, M.A. Skoryk, V.I. Nevmerzhytskyi, and V.I. Bondarchuk, New Approach for Manufacturing Ti-6Al-4V+40% TiC Metal-Matrix Composites by 3D Printing Using Conic Electron Beam and Cored Wire. Pt. 2: Layered MMC/Alloy Materials, Their Main Characteristics, and Possible Application as Ballistic Resistant Materials, Prog. Phys. Met., 24, No. 4: 741-763 (2023); https://doi.org/10.15407/ufm.24.04.741
- 54. M.O. Vasylyev, B.M. Mordyuk, and S.M. Voloshko, Wire-Feeding Based Additive Manufacturing of the Ti-6Al-4V Alloy. Part I. Microstructure, *Prog. Phys. Met.*, 24, No. 1: 5-37 (2023); https://doi.org/10.15407/ufm.24.01.005
- 55. M.O. Vasylyev, B.M. Mordyuk, and S.M. Voloshko, Wire-Feeding Based Additive Manufacturing of the Ti-6Al-4V Alloy. Pt. II. Mechanical Properties, *Progress in Physics of Metals*, 24, No. 1: 38-74 (2023); https://doi.org/10.15407/ufm.24.01.038

Received 11.03.2025 Final version 04.08.2025

O.I. Дехтяр 1 , Я. Янішевський 2 , П.Є. Марковський 1

¹Інститут металофізики ім. Г.В. Курдюмова НАН України, бульв. Академіка Вернадського, 36, 03142 Київ, Україна

² Військовий технічний університет ім. Ярослава Данбровського, вул. ген. Сильвестра Каліського, 2, 00-908, Варшава, Польща

ЗАКОНОМІРНОСТІ МЕХАНІЗМІВ ДЕФОРМАЦІЇ ТА ДЕФОРМАЦІЙНОГО ЗМІЦНЕННЯ ТИТАНОВИХ СПЛАВІВ І МЕТАЛОМАТРИЧНИХ КОМПОЗИТІВ НА ОСНОВІ АНАЛІЗУ ЕКСПЕРИМЕНТАЛЬНИХ РЕЗУЛЬТАТІВ КВАЗІСТАТИЧНИХ І ДИНАМІЧНИХ СТИСНЕНЬ

Проаналізовано деформаційну поведінку сплавів на основі титану та їхніх композитів за квазістатичного та високошвидкісного стиснень за методикою, розробленою В.Ф. Моїсеєвим та його колегами для аналізу кривих деформації, одержаних на розтяг. Описаний у цьому огляді підхід застосовано для оброблення і подальшого аналізу численних кривих випробувань стисненням, одержаних у квазістатичних

експериментах та експериментах із високою швидкістю деформування сплавів на основі титану і його композитів з різними складом та початковою мікроструктурою. Переконливо показано, що метод за Моїсеєвим також може бути успішно застосований для аналізу поведінки сплавів під час стиснення. Порівняння одержаних даних з результатами структурних досліджень дало змогу в більшості випадків виявити механізми деформування та зміцнення титанових сплавів у широкому діапазоні швидкостей стиснення. Встановлено, що залежно від типу та морфології вихідної структури деформація та зміцнення під час стиснення можуть контролюватися а- чи в-фазою або обома ними одночасно. Розглянуто вплив рівня легування β-стабілізаторами та введення в титанову матрицю зміцнювальних дисперсних високомодульних частинок. Виявлено, що механізм зміцнення часто відрізняється за умов квазістатичного та динамічного стиснень. Крім того, за високої швидкості деформування стисненням він може бути різним для першого та наступних етапів деформування, яке має коливний характер. Запропоновано фізичне пояснення ефектів, виявлених під час квазістатичного та динамічного стиснень розглянутих титанових матеріалів.

Ключові слова: титан, титанові сплави, композити з титановою матрицею, випробування стисненням, квазістатичне та динамічне деформування, механізм деформації.